

# Systematic analysis of strange single heavy baryons $\Xi_c$ and $\Xi_b$

Zhen-Yu Li<sup>1,\*</sup>, Guo-Liang Yu<sup>2,†</sup>, Zhi-Gang Wang<sup>2,‡</sup>, Jian-Zhong Gu<sup>3</sup>, and Jie Lu<sup>2</sup>

<sup>1</sup> *School of Physics and Electronic Science,*

*Guizhou Education University, Guiyang 550018, China*

<sup>2</sup> *Department of Mathematics and Physics,*

*North China Electric Power University, Baoding 071003, China*

<sup>3</sup> *China Institute of Atomic Energy, Beijing 102413, China*

(Dated: December 8, 2022)

Motivated by the experimental progress in the study of heavy baryons and the theoretical work of Ebert *et al.*, we investigate the mass spectra of strange single heavy baryons systematically. In the calculation of the Hamiltonian matrix elements, the relativistic quark model and the infinitesimally shifted Gaussian basis function method are employed. The results show that the  $\lambda$ -mode appears lower in energy than other excited modes for a given excited state  $nL(J^P)$ . Considering this feature, we perform a systematic study of the mass spectra of the  $\Xi_c$  ( $\Xi'_c$ ) and  $\Xi_b$  ( $\Xi'_b$ ) families. It is shown that the experimental data can be well reproduced by the predicted masses. By analyzing the root mean square radii and radial probability density distributions of the wave functions of the strange single heavy baryons, we set the upper limit of the mass spectrum and constrain the number of members for each heavy baryon family. Meanwhile, the mass spectra allow us to successfully construct the Regge trajectories in the  $(J, M^2)$  plane. We also preliminarily assign of the quantum numbers to the recently observed excited strange single heavy baryons, including  $\Xi_c(3055)$ ,  $\Xi_c(3080)$ ,  $\Xi_c(2930)$ ,  $\Xi_c(2923)$ ,  $\Xi_c(2939)$ ,  $\Xi_c(2965)$ ,  $\Xi_c(2970)$ ,  $\Xi_c(3123)$ ,  $\Xi_b(6100)$ ,  $\Xi_b(6227)$ ,  $\Xi_b(6327)$  and  $\Xi_b(6333)$ . At last, the spectral structure of the strange single heavy baryons is shown, from which one could get a bird's-eye view of the mass spectra. Accordingly, we predict several new baryons that might be observed in forthcoming experiments.

Key words: Single heavy baryons, Mass spectra, Relativistic quark model.

PACS numbers: 13.25.Ft; 14.40.Lb

## I. Introduction

In recent years, many single heavy baryons have been observed in experiments, and the mass spectra of single heavy baryon families have become more and more abundant [1–31]. Under this background,

---

\*Electronic address: zhenyvli@163.com

†Electronic address: yuguoliang2011@163.com

‡Electronic address: zgwang@aliyun.com

searching for new heavy baryons and completing the heavy baryon spectra provoked many interests in the field of hadron physics. At the same time, such a wealth of experimental data gives theorists an opportunity to test the validity of current theoretical frameworks. Additionally, this is also a good time to carry out a systematic and precise calculation with some theoretical methods (models), so as to promote the consistency between the experiments and theories.

As an important part of the heavy baryons spectra, the strange single heavy baryon ( $\Xi_Q$ ) families including  $\Xi_c$  ( $\Xi'_c$ ) [1–15] and  $\Xi_b$  ( $\Xi'_b$ ) [17–27], are being established step by step with the cooperative efforts from both experimentalists and theorists. Up to now, more than a dozen of  $\Xi_Q$  baryons have been recorded in the latest particle data group (PDG) [30], even though the quantum numbers  $J^P$  of some members are still not confirmed, for instance,  $\Xi_c(3055)$ ,  $\Xi_c(3080)$  and  $\Xi_c(6227)$ . In addition, several new  $\Xi_Q$  baryons have been observed in experiment, such as  $\Xi_c(3123)$  [5],  $\Xi_c(2930)$  [13],  $\Xi_c(2923)$ ,  $\Xi_c(2939)$ ,  $\Xi_c(2964)$  [14],  $\Xi_b(6327)$  and  $\Xi_b(6333)$  [27]. Once their  $J^P$  quantum numbers are identified, they will be accommodated in the  $\Xi_Q$  families as well. Accordingly, there have been a lot of theoretical studies on these baryons in recent years, such as  $\Xi_c(3055)$  [32–36],  $\Xi_c(3080)$  [36–39],  $\Xi_c(2923)^0$  (including  $\Xi_c(2939)^0$  and  $\Xi_c(2965)^0$ ) [40],  $\Xi_c(2930)^0$  [41],  $\Xi_c(2970)$  [42–47],  $\Xi_c(3123)$  [48],  $\Xi_b(6227)$  [49–53],  $\Xi_b(6100)$  [54, 55] and  $\Xi_b(6327)$  ( $\Xi_b(6333)$ ) [56]. It is believed that more strange single heavy baryons are to be discovered in the near future. In order to identify their quantum numbers and assign them suitable positions in the mass spectra, it is necessary to systematically investigate their spectroscopies.

For a definite state of baryons, its mass and strong decay behavior are commonly studied by the following theoretical methods: The quark potential model in the heavy quark-light diquark picture [48, 57–60], relativistic quark model [61, 62], harmonic oscillator quark model [40], constituent quark model [63–66], chiral quark model [32, 41, 49, 56], chiral perturbation theory [67–71], relativistic flux tube model [42], Bethe-Salpeter formalism [72], effective Lagrangian approach [50],  $^3P_0$  decay model [73–80], lattice QCD [81–84], bound state picture [85], light cone QCD sum rules [86–95], and QCD sum rules method [96–105].

It is particularly worth mentioning that Ebert *et al.* [57, 58] put forward a heavy quark-light diquark picture in the framework of a QCD-motivated relativistic quark model, in which an initial three-body problem is reduced to a two-step two-body problem. According to this picture, the quantum states can be labeled with  $nL(J^P)$ , where  $n$  and  $L$  denote the radial quantum number and the orbital quantum number between the heavy quark and light quark pair, respectively. They systematically studied the spectroscopy and Regge trajectories of heavy baryons, and have achieved a great success in predicting new singly heavy baryons. Because the excited states in the heavy quark-light diquark picture is very similar to those of the  $\lambda$ -mode in a three-quark system [63], it would be interesting to investigate the difference in mass spectra between the heavy quark-light diquark picture and the  $\lambda$ -mode in a real three-quark system.

In the 1980s, Godfrey and Isgur developed a relativistic quark model by which they studied mass spectra of mesons [106]. Then, Capstick and Isgur extended it to a baryon model [61] and studied baryon spectra preliminarily. In the baryon model, the Hamiltonian contains almost all of the interactions between quarks, which is expected to give accurate calculations for heavy baryon spectra. Due to the limited power of computers at the time, however, the baryon model did not realize its greater potential.

In recent decades, the Gaussian expansion method (GEM) and the infinitesimally-shifted Gaussian (ISG) basis functions [107] have been successfully applied to few-body systems in nuclear physics. They were first introduced in the study of heavy baryons [63] in 2015 and then applied to analyze furthermore heavy baryons [64, 65], tetraquarks [108–110] and pentaquark resonances [111]. The ISG method can improve the accuracy and efficiency of calculation in a few-body system effectively.

Inspired by the above discussion, we try to combine the baryon model [61] with the ISG method [107], so as to investigate the strange single heavy baryon spectra of real three-quark systems. For the excited states, we would only focus on the  $\lambda$ -mode and compare the results with those of the heavy quark-light diquark picture and the relevant experimental data as well. The present work is a preliminary attempt to systematically investigate strange single heavy baryon spectra and the combined method is promising to be used in the study of all the multi-quark systems, including the exotic ones [112–116].

This paper is organized as follows. In Sect.II, we briefly describe the methods used in the theoretical calculations, mainly including the baryon model and the GEM(ISG) method. In Sect.III, we present the root mean square radii and the mass spectra of the  $\Xi_Q$  baryons, analyze the radial probability distributions, and construct the Regge trajectories. On these bases, we perform a detailed analysis of the baryons that have been of interest recently. And Sect.IV is reserved for our conclusions.

## II. Phenomenological methods adopted in this work

In our series of papers on the heavy baryons, we apply the baryon model [61] to investigate the mass spectra. The relevant technical details can be found in our previous paper [62]. Therefore, in this section, we only give an outline of the phenomenological methods.

### 2.1 GI model and Jacobi coordinates

The baryon model is based on the hypothesis that baryons may be approximately described in terms of center-of-mass (CM) frame valence-quark configurations, the dynamics of which are governed by a Hamiltonian with a one-gluon exchange dominant component at short distances and with a confinement implemented by a flavor-independent Lorentz-scalar interaction [61]. For a three-quark

system the Hamiltonian reads,

$$H = H_0 + V, \quad (1)$$

$$H_0 = \sum_{i=1}^3 (p_i^2 + m_i^2)^{1/2}, \quad (2)$$

$$V = \sum_{i < j} (\tilde{H}_{ij}^{conf} + \tilde{H}_{ij}^{so} + \tilde{H}_{ij}^{hyp}), \quad (3)$$

where  $\tilde{H}_{ij}^{conf}$ ,  $\tilde{H}_{ij}^{so}$  and  $\tilde{H}_{ij}^{hyp}$  are the confinement, spin-orbit and hyperfine interactions, respectively. The confinement item includes one-gluon exchange potentials and the linear confined potentials. Due to the relativistic effect, the interactions should be modified with CM momentum-dependent factors. It is worth noting that the forms of the interactions in this paper have been rearranged for ease of use [108, 117]. The interactions are decomposed as follows:

$$\tilde{H}_{ij}^{conf} = G'_{ij}(r) + \tilde{S}_{ij}(r), \quad (4)$$

$$\tilde{H}_{ij}^{so} = \tilde{H}_{ij}^{so(v)} + \tilde{H}_{ij}^{so(s)}, \quad (5)$$

$$\tilde{H}_{ij}^{hyp} = \tilde{H}_{ij}^{tensor} + \tilde{H}_{ij}^c, \quad (6)$$

with

$$\tilde{H}_{ij}^{so(v)} = \frac{\mathbf{S}_i \cdot \mathbf{L}_{ij}}{2m_i^2 r_{ij}} \frac{\partial \tilde{G}_{ij}^{so(v)}}{\partial r_{ij}} + \frac{\mathbf{S}_j \cdot \mathbf{L}_{ij}}{2m_j^2 r_{ij}} \frac{\partial \tilde{G}_{ij}^{so(v)}}{\partial r_{ij}} + \frac{(\mathbf{S}_i + \mathbf{S}_j) \cdot \mathbf{L}_{ij}}{m_i m_j r_{ij}} \frac{\partial \tilde{G}_{ij}^{so(v)}}{\partial r_{ij}}, \quad (7)$$

$$\tilde{H}_{ij}^{so(s)} = -\frac{\mathbf{S}_i \cdot \mathbf{L}_{ij}}{2m_i^2 r_{ij}} \frac{\partial \tilde{S}_{ij}^{so(s)}}{\partial r_{ij}} - \frac{\mathbf{S}_j \cdot \mathbf{L}_{ij}}{2m_j^2 r_{ij}} \frac{\partial \tilde{S}_{ij}^{so(s)}}{\partial r_{ij}}, \quad (8)$$

$$\tilde{H}_{ij}^{tensor} = -\frac{\mathbf{S}_i \cdot \mathbf{r}_{ij} \mathbf{S}_j \cdot \mathbf{r}_{ij} / r_{ij}^2 - \frac{1}{3} \mathbf{S}_i \cdot \mathbf{S}_j}{m_i m_j} \times \left( \frac{\partial^2}{\partial r_{ij}^2} - \frac{1}{r_{ij}} \frac{\partial}{\partial r_{ij}} \right) \tilde{G}_{ij}^t, \quad (9)$$

$$\tilde{H}_{ij}^c = \frac{2\mathbf{S}_i \cdot \mathbf{S}_j}{3m_i m_j} \nabla^2 \tilde{G}_{ij}^c. \quad (10)$$

The modified terms in Eqs. (4), (7), (8), (9) and (10) read,

$$G'_{ij} = \left(1 + \frac{p_{ij}^2}{E_i E_j}\right)^{\frac{1}{2}} \tilde{G}_{ij}(r_{ij}) \left(1 + \frac{p_{ij}^2}{E_i E_j}\right)^{\frac{1}{2}}, \quad (11)$$

$$\tilde{G}_{ij}^{so(v)} = \left(\frac{m_i m_j}{E_i E_j}\right)^{\frac{1}{2} + \epsilon_{so(v)}} \tilde{G}_{ij}(r_{ij}) \left(\frac{m_i m_j}{E_i E_j}\right)^{\frac{1}{2} + \epsilon_{so(v)}}, \quad (12)$$

$$\tilde{S}_{ii}^{so(s)} = \left(\frac{m_i m_i}{E_i E_i}\right)^{\frac{1}{2} + \epsilon_{so(s)}} \tilde{S}_{ij}(r_{ij}) \left(\frac{m_i m_i}{E_i E_i}\right)^{\frac{1}{2} + \epsilon_{so(s)}}, \quad (13)$$

$$\tilde{G}_{ij}^t = \left(\frac{m_i m_j}{E_i E_j}\right)^{\frac{1}{2} + \epsilon_t} \tilde{G}_{ij}(r_{ij}) \left(\frac{m_i m_j}{E_i E_j}\right)^{\frac{1}{2} + \epsilon_t}, \quad (14)$$

$$\tilde{G}_{ij}^c = \left(\frac{m_i m_j}{E_i E_j}\right)^{\frac{1}{2} + \epsilon_c} \tilde{G}_{ij}(r_{ij}) \left(\frac{m_i m_j}{E_i E_j}\right)^{\frac{1}{2} + \epsilon_c}, \quad (15)$$

where  $E_i = \sqrt{m_i^2 + p_{ij}^2}$  is the relativistic kinetic energy, and  $p_{ij}$  is the momentum magnitude of either of the quarks in the CM frame of the  $ij$  quark subsystem [108].

$\tilde{G}_{ij}(r_{ij})$  and  $\tilde{S}_{ij}(r_{ij})$  are obtained by the smearing transformations of the one-gluon exchange potential  $G(r) = -\frac{4\alpha_s(r)}{3r}$  and linear confinement potential  $S(r) = br + c$ , respectively,

$$\tilde{G}_{ij}(r_{ij}) = \mathbf{F}_i \cdot \mathbf{F}_j \sum_{k=1}^3 \frac{2\alpha_k}{\sqrt{\pi}r_{ij}} \int_0^{\tau_{kij}r_{ij}} e^{-x^2} dx, \quad (16)$$

$$\tilde{S}_{ij}(r_{ij}) = -\frac{3}{4}\mathbf{F}_i \cdot \mathbf{F}_j \left\{ br_{ij} \left[ \frac{e^{-\sigma_{ij}^2 r_{ij}^2}}{\sqrt{\pi}\sigma_{ij}r_{ij}} + \left(1 + \frac{1}{2\sigma_{ij}^2 r_{ij}^2}\right) \frac{2}{\sqrt{\pi}} \int_0^{\sigma_{ij}r_{ij}} e^{-x^2} dx \right] + c \right\}, \quad (17)$$

with

$$\tau_{kij} = \frac{1}{\sqrt{\frac{1}{\sigma_{ij}^2} + \frac{1}{\gamma_k^2}}}, \quad (18)$$

$$\sigma_{ij} = \sqrt{s^2 \left( \frac{2m_i m_j}{m_i + m_j} \right)^2 + \sigma_0^2 \left( \frac{1}{2} \left( \frac{4m_i m_j}{(m_i + m_j)^2} \right)^4 + \frac{1}{2} \right)}. \quad (19)$$

Here  $\alpha_k$  and  $\gamma_k$  are constants.  $\mathbf{F}_i \cdot \mathbf{F}_j$  stands for the inner product of the color matrices of quarks  $i$  and  $j$ .  $\mathbf{F}$  includes 8 components (the so-called Gell-mann matrices), which can be written as

$$F_n = \begin{cases} \frac{\hat{\lambda}_n}{2}, & \text{for quarks,} \\ -\frac{\hat{\lambda}_n^*}{2}, & \text{for antiquarks,} \end{cases} \quad (20)$$

with  $n = 1, \dots, 8$ . All of the parameters in these formulas are cited from reference [61], apart from two parameters associated with the linear potential [62].

To represent the internal motion of quarks in a few-body system, one commonly introduces the Jacobi coordinates. As shown in Fig.1, there are totally three channels of Jacobi coordinates for the three-body system. The corresponding Jacobi coordinates are defined as

$$\boldsymbol{\rho}_i = \mathbf{r}_j - \mathbf{r}_k, \quad (21)$$

$$\boldsymbol{\lambda}_i = \mathbf{r}_i - \frac{m_j \mathbf{r}_j + m_k \mathbf{r}_k}{m_j + m_k}, \quad (22)$$

where  $i, j, k = 1, 2, 3$  (or replace their positions in turn).  $\mathbf{r}_i$  and  $m_i$  denote the position vector and the mass of the  $i$ th quark, respectively.

In order to be consistent with reference [58], we perform the calculations based on the channel 3. In this case, the 3rd quark is just the heavy quark, which is consistent with the heavy quark limit [118, 119]. What is more,  $\mathbf{l}_{\rho 3}$  (denoted in short as  $\mathbf{l}_\rho$ ) is clearly defined as the orbital angular momentum between the light quarks, and  $\mathbf{l}_{\lambda 3}$  (denoted in short as  $\mathbf{l}_\lambda$ ) represents the one between the heavy quark and the light-quark pair.

## 2.2 The heavy quark limit and wave function

In the heavy quark limit [118, 119], the heavy quark within the heavy baryon system is decoupled from the two light quarks. With the requirement of the flavor SU(3) subgroups for the light quarks,

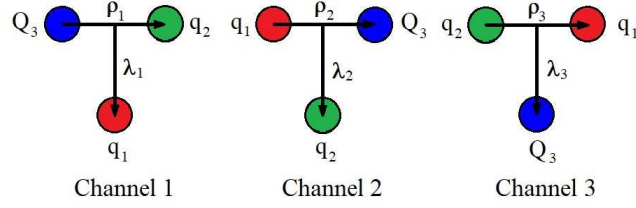


FIG. 1: (Color online) Jacobi coordinates for the three-body system. We denote the heavy quark as the 3rd particle in the case of single heavy baryons.

the baryons belong to either a sextet ( $6_F$ ) of flavor symmetric states  $\Xi'_Q$  with the total spin of the light quarks  $s = 1$ , or an antitriplet ( $\bar{3}_F$ ) of the flavor antisymmetric states  $\Xi_Q$  with  $s = 0$ , being the  $\lambda$ -mode ( $l_\rho = 0$ ) used in this work (see subsection 3.1). This guarantees the antisymmetry of the total wave function, because the color wave function is always asymmetric for a baryon. The flavor wave functions of strange single heavy baryons are written as,

$$\begin{aligned}\Xi'_Q &= \frac{1}{\sqrt{2}}(qq_s + q_s q)Q, \\ \Xi_Q &= \frac{1}{\sqrt{2}}(qq_s - q_s q)Q.\end{aligned}\tag{23}$$

Here  $q$  denotes light quark  $u$  or  $d$ , and  $Q$  is  $c$  or  $b$  quark.  $q_s$  is strange quark. For a quantum state with specified angular momenta in this work, the spatial wave function is combined with the spin function as follow.

$$\begin{aligned}|l_\rho \ l_\lambda \ L \ s \ j \ J \ M_J\rangle &= \sum_{m_{s3}=-1/2}^{1/2} \sum_{m_j=-j}^j \sum_{M_L=-L}^L \sum_{m_s=-s}^s \sum_{m_{s1}=-1/2}^{1/2} \sum_{m_{s2}=-1/2}^{1/2} \sum_{m_\rho=-l_\rho}^{l_\rho} \sum_{m_\lambda=-l_\lambda}^{l_\lambda} \\ &\times \langle j \ m_j \ s_3 \ m_{s3} | j \ s_3 \ J \ M_J \rangle \times \langle L \ M_L \ s \ m_s | L \ s \ j \ m_j \rangle \\ &\times \langle s_1 \ m_{s1} \ s_2 \ m_{s2} | s_1 \ s_2 \ s \ m_s \rangle \times \langle l_\rho \ m_\rho \ l_\lambda \ m_\lambda | l_\rho \ l_\lambda \ L \ M_L \rangle \\ &\times |l_\rho \ m_\rho\rangle \otimes |l_\lambda \ m_\lambda\rangle \otimes |s_1 \ m_{s1}\rangle \otimes |s_2 \ m_{s2}\rangle \otimes |s_3 \ m_{s3}\rangle,\end{aligned}\tag{24}$$

with  $\mathbf{J} = \mathbf{j} + \mathbf{s}_3$ ,  $\mathbf{j} = \mathbf{L} + \mathbf{s}$ ,  $\mathbf{s} = \mathbf{s}_1 + \mathbf{s}_2$ ,  $\mathbf{L} = \mathbf{l}_\rho + \mathbf{l}_\lambda$ .  $l_\rho$ ,  $l_\lambda$ ,  $L$ ,  $s$ ,  $j$ ,  $J$  and  $M_J$  are the quantum numbers which characterize a given quantum state in theory.

### 2.3 GEM and ISG

In calculations, the spatial wave function  $|l_\rho \ m_\rho\rangle \otimes |l_\lambda \ m_\lambda\rangle$  in formula (24) should be expanded in a set of basis functions. Naturally, one of the candidates is the simple harmonic oscillator(SHO) basis for its good orthogonality. However, the completeness of the SHO is not rigorous in calculations because

a truncated set has to be used [61, 106]. One can commonly enlarge the harmonic-oscillator-based space to asymptotically satisfy the completeness. Nevertheless, the computation time will increase significantly. Compared to the SHO basis functions, the advantage of the Gaussian basis functions is that they can form an approximately complete set in a finite coordinate space.

Following formula (24), the spatial wave function is expanded in terms of a set of Gaussian basis functions,

$$|l_\rho m_\rho\rangle \otimes |l_\lambda m_\lambda\rangle = \sum_{n_\rho=1}^{n_{max}} \sum_{n_\lambda=1}^{n_{max}} c_{n_\rho n_\lambda} |n_\rho l_\rho m_\rho\rangle^G \otimes |n_\lambda l_\lambda m_\lambda\rangle^G, \quad (25)$$

where the Gaussian basis function  $|nlm\rangle^G$  is commonly written in position space as [107]

$$\begin{aligned} \phi_{nlm}^G(\mathbf{r}) &= \phi_{nl}^G(r) Y_{lm}(\hat{\mathbf{r}}), \\ \phi_{nl}^G(r) &= N_{nl} r^l e^{-\nu_n r^2}, \\ N_{nl} &= \sqrt{\frac{2^{l+2} (2\nu_n)^{l+3/2}}{\sqrt{\pi} (2l+1)!!}}, \end{aligned} \quad (26)$$

or in momentum space as

$$\begin{aligned} \phi_{nlm}'^G(\mathbf{p}) &= \phi_{nl}'^G(p) Y_{lm}(\hat{\mathbf{p}}), \\ \phi_{nl}'^G(p) &= N_{nl}' p^l e^{-\frac{p^2}{4\nu_n}}, \\ N_{nl}' &= (-i)^l \sqrt{\frac{2^{l+2}}{\sqrt{\pi} (2\nu_n)^{l+3/2} (2l+1)!!}}, \end{aligned} \quad (27)$$

with

$$\begin{aligned} \nu_n &= \frac{1}{r_n^2}, \\ r_n &= r_1 a^{n-1} \quad (n = 1, 2, \dots, n_{max}). \end{aligned} \quad (28)$$

$r_1$ ,  $a$ , and  $n_{max}$  are the Gaussian size parameters in the geometric progression for numerical calculations, and the final results are stable and independent of these parameters within an approximately complete set in a sufficiently large space.

The Gaussian basis functions are non-orthogonal, which leads to a generalized matrix eigenvalue problem,

$$\sum_{\kappa, \kappa'=1}^{\kappa_{max}} [H_{\kappa\kappa'} - E \tilde{N}_{\kappa\kappa'}] C_{\kappa'} = 0, \quad (29)$$

with

$$\begin{aligned} \tilde{N}_{\kappa\kappa'} &= \langle \phi_{n_\rho l_\rho m_\rho}^G | \phi_{n_{\rho'} l_{\rho'} m_{\rho'}}^G \rangle \times \langle \phi_{n_\lambda l_\lambda m_\lambda}^G | \phi_{n_{\lambda'} l_{\lambda'} m_{\lambda'}}^G \rangle \\ &= \left( \frac{2\sqrt{\nu_{n_\rho} \nu_{n_{\rho'}}}}{\nu_{n_\rho} + \nu_{n_{\rho'}}} \right)^{l_\rho+3/2} \times \left( \frac{2\sqrt{\nu_{n_\lambda} \nu_{n_{\lambda'}}}}{\nu_{n_\lambda} + \nu_{n_{\lambda'}}} \right)^{l_\lambda+3/2}, \end{aligned} \quad (30)$$

where  $\kappa = 1, 2, \dots, \kappa_{max}$ ,  $\kappa_{max} = n_{max} \times n_{max}$  and  $c_\kappa = c_{n_\rho n_\lambda}$ .  $H$  and  $E$  denote the Hamiltonian and the eigenvalue, respectively.

In the calculation of Hamiltonian matrix elements of three-body systems, particularly when complicated interactions are employed, integrations over all of the radial and angular coordinates become laborious even with the Gaussian basis functions. This process can be simplified by introducing the ISG basis functions. The technical details can be found in references [62, 107].

Note that there are two key issues in our mass spectrum calculations. The first is the Hamiltonian calculation which starts with the two-quark interactions, and is different from that of the quark potential model in the heavy quark-light diquark picture [58]; The second is the definition of a baryon state. Besides the flavor wave function of  $\bar{3}_F$  or  $6_F$ , the spin and spatial wave functions in this work are defined by  $|l_\rho l_\lambda L s j J M_J\rangle$  as shown in formula (24). In fact, there exists another scheme written as  $|l_\rho l_\lambda L s S J M_J\rangle$  ( $L$ - $S$  coupling [107]), which may be transformed into  $|l_\rho l_\lambda L s j J M_J\rangle$  ( $j$ - $s$  coupling) by means of Racah coefficients. In addition, the  $j$ - $s$  coupling scheme has also been widely employed in the strong decay calculations of heavy baryons by the  $^3P_0$  model [77].

### III. Numerical results and discussions

#### 3.1 Numerical stabilities and the $\lambda$ -mode

In order to obtain stable numerical solutions of the generalized matrix eigenvalue problem, the Gaussian size parameters set  $\{n_{max}, r_1, r_{n_{max}}\}$  should be optimized. For the Gaussian functions which are a set of non-orthogonal bases in a finite coordinate space, the number of the bases should be located within a reasonable range. As shown in Fig.2, the numerical stability is achieved when the dimension parameter  $n_{max}$  falls in the range of  $9 \sim 14$ , with  $r_1 = 0.18\text{GeV}^{-1}$  and  $r_{n_{max}} = 15\text{GeV}^{-1}$ .  $n_{max} = 10$  is finally adopted in this work, with which both the computation efficiency and accuracy are actually satisfied [62].

As usual,  $nL(J^P)$  is used to describe a baryon state in this work. If angular momentum  $L \neq 0$ , there exist several  $|l_\rho l_\lambda L s j J M_J\rangle$  states under the condition of  $\mathbf{L} = \mathbf{l}_\rho + \mathbf{l}_\lambda$ . They may be divided into the following three modes: (1) The  $\rho$ -mode with  $l_\rho \neq 0$  and  $l_\lambda = 0$ ; (2) The  $\lambda$ -mode with  $l_\rho = 0$  and  $l_\lambda \neq 0$ ; (3) The  $\lambda$ - $\rho$  mixing mode with  $l_\rho \neq 0$  and  $l_\lambda \neq 0$ . In general, the real mass spectrum should be obtained by considering the mixing between these modes. In order to be consistent with the heavy quark-light diquark picture [58], we ignore this mixing. Note that the quantum states most likely to be observed experimentally should be those with lower energies.

In this subsection, the excitation energies of the  $1P(\frac{1}{2}^-, \frac{3}{2}^-)_{j=1}$  states of  $\bar{3}_F$  as functions of  $m_Q$  are investigated, where the dependence of excitation energies on  $m_Q$  of the  $\lambda$ -mode is compared with



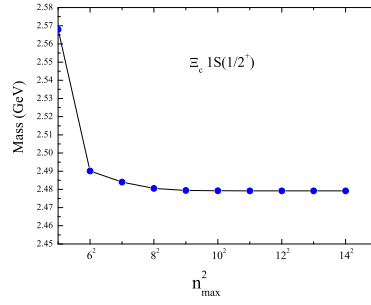


FIG. 2: (Color online) Numerical stability of  $\Xi_c 1S(\frac{1}{2}^+)$  mass with respect to the dimension parameter  $n_{max}$ .

that of the  $\rho$ -mode. As shown in Fig.3, the  $\lambda$ -mode and the  $\rho$ -mode are clearly separated when  $m_Q$  increases from 0.2 GeV to 5.0 GeV. In general, the excitation energies of the  $\lambda$ -mode are lower than those of the  $\rho$ -mode. In the case of  $6_F$ , we come to the same conclusion when  $m_Q > 1.5\text{GeV}$  as shown in Fig.4.

Generally, the  $\lambda$ -mode appears lower in energy than the other two modes and they do not mix with each other in the heavy quark limit for single heavy baryons [62, 63]. Actually, the  $\lambda$ -mode has been applied widely in the study of heavy baryon strong decays [27, 35, 54, 119]. Therefore, we only calculate the  $\lambda$ -mode in  $\Xi_Q$  baryons. Additionally, the excitation energies of the  $\frac{1}{2}^-$  and  $\frac{3}{2}^-$  states are closer to each other with increasing  $m_Q$  as shown in Figs. 3 and 4, which is consistent with the heavy quark spin symmetry [120].

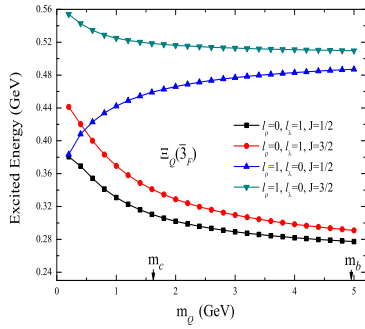


FIG. 3: (Color online) The dependence of excitation energies on  $m_Q$  for different modes of  $\Xi_Q$ . The black and red curves represent the  $\lambda$ -mode. The blue and green ones denote the  $\rho$ -mode.

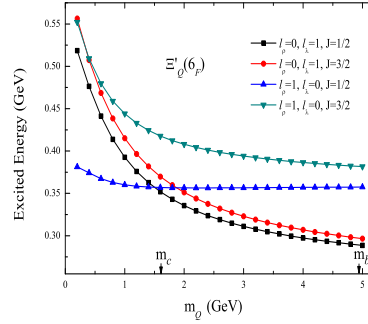


FIG. 4: (Color online) The excitation energies versus  $m_Q$  for different modes of  $\Xi'_Q$ . Note that the black curve is lower than the blue one with  $m_Q > 1.5\text{GeV}$  and the red curve is overall lower than the green one ( $m_c = 1.628\text{ GeV}$  and  $m_b = 4.977\text{ GeV}$  are taken in this work).

### 3.2 Mass spectra, root mean square radius and radial probability density distribution

In this subsection, the root mean square radii, radial probability density distributions and the mass spectra of strange single heavy baryons are presented. For convenience, the relevant experimental data are given together. The detailed results are listed in Tables I-VI (see the appendix). There are a total of four families for  $\Xi_Q$  baryons in this work, namely  $\Xi_c$ ,  $\Xi'_c$ ,  $\Xi_b$  and  $\Xi'_b$ . The mass spectra of excited states with quantum numbers up to  $n = 4$  and  $L = 4$  are displayed. There have been a lot of other theoretical works on this subject [36, 38, 50, 121, 122]. Among them, Ebert *et al.* have studied the heavy baryon spectra with a quark potential model in the heavy quark-light diquark picture [58]. As an important reference, their numerical results are also placed in the tables.

Through the analysis of these calculated results, some general features of the mass spectra are summarized as follows:

- (1) The GI model gives the same mass for  $\Xi_c^+$  and  $\Xi_c^0$ , due to the isospin symmetry of  $u$  and  $d$  quarks in this model.
- (2)  $\Xi_Q$  is lower than  $\Xi'_Q$  in energy. This feature has been recognized in light baryons where the highly orbitally excited states have an antisymmetric structure which minimizes the energy [123].
- (3) For the spin-doublet states, the energy of the  $J = j + \frac{1}{2}$  state is higher than that of the  $J = j - \frac{1}{2}$  state. This is also a general rule in hadronic physics.
- (4) The mass splitting of spin-doublet states becomes smaller with increasing  $L$ . For example, Table I shows the mass differences of the spin-doublets of  $1P$ -,  $1D$ -,  $1F$ -, and  $1G$ -wave are 30 MeV, 13 MeV, 5 MeV, and 1 MeV, respectively.
- (5) For the same  $L$ , the mass splitting hardly changes with the increase of  $j$ . For example, Tables II and III show the mass differences of  $1D$  doublets with  $j = 1, 2, 3$  are 10 MeV, 10 MeV and 13 MeV, respectively.
- (6) The mass difference between the two adjacent radial excited states gradually decreases with increasing  $n$ , which is clearly different from that given by Ebert *et al.*
- (7) The above six features are roughly the same for  $\Xi_c$  ( $\Xi'_c$ ) and  $\Xi_b$  ( $\Xi'_b$ ) families, which is consistent with the heavy quark flavor symmetry [120].

On the other hand, the calculated root mean square radii and radial probability density distributions carry important information. For a three-quark system, the radial probability densities  $\omega(r_\rho)$  and  $\omega(r_\lambda)$  can be defined as follows,

$$\begin{aligned}\omega(r_\rho) &= \int |\Psi(\mathbf{r}_\rho, \mathbf{r}_\lambda)|^2 d\mathbf{r}_\lambda d\Omega_\rho, \\ \omega(r_\lambda) &= \int |\Psi(\mathbf{r}_\rho, \mathbf{r}_\lambda)|^2 d\mathbf{r}_\rho d\Omega_\lambda,\end{aligned}\tag{31}$$

where  $\Omega_\rho$  and  $\Omega_\lambda$  are the solid angles spanned by vectors  $\mathbf{r}_\rho$  and  $\mathbf{r}_\lambda$ , respectively. From Figs.5-7 and tables I-VI, one can find some interesting properties of the root mean square radii and the radial probability density distributions.

(1) For the  $1L$  states, the difference of their  $\langle r_\rho^2 \rangle^{1/2}$  values is relatively small. While their  $\langle r_\lambda^2 \rangle^{1/2}$  values become larger with increasing  $L$ . In Figs.5 and 6, for the  $r_\rho$  modes, the radial probability versus the radial distance  $r$  with  $r_\rho$  (black lines) changes a little with  $L$ . But, for the  $r_\lambda$  modes, the peak of the probability is significantly shifted outward with increasing  $L$ .

(2) For the same  $L$  states,  $\langle r_\rho^2 \rangle^{1/2}$  and  $\langle r_\lambda^2 \rangle^{1/2}$  generally become larger with increasing  $n$ . And the peaks of their probability densities are generally shifted outward, as shown in Fig.7.

(3) The shapes of the eight black lines in Fig.5 are almost as same as those in Fig.6. Accordingly, the values of  $\langle r_\rho^2 \rangle^{1/2}$  for the same state are almost the same for  $\Xi_c(\Xi'_c)$  and  $\Xi_b(\Xi'_b)$  families. This reflects the fact that the configurations of the two light quarks in the single charm baryons and in the single bottom baryons are similar to each other.

(4) As shown in tables I-VI, the root mean square radii of those baryons which have been experimentally well established are generally less than 0.8 fm.

When the root mean square radius becomes larger, the radial probability distribution of the wave function appears more outwardly extended, and the baryons become even looser. Generally speaking, the root mean square radius of a compact baryon is within a threshold, which is of help to estimate the upper limit of the mass spectrum and constrain the number of members for each heavy baryon family. For example, there should be only six members in the  $\Xi_c$  family and the maximum mass should be no more than 3076 MeV, if we set the threshold to be 0.9 fm (see Table IX in the appendix).

### 3.3 Regge trajectories

Regge theory is based on Lorentz invariance, unitarity and analyticity of the scattering matrix and serves as a fundamental theory of strong interactions at very high energies and still an indispensable tool in phenomenological studies[124, 125] due to its generality although the Regge's original work does not involve quarks and gluons and even a confining potential. Chew and Frautschi applied the theory to the case of strong interactions and found mesons and baryons lie on linear trajectories of the  $(J, M^2)$  plane[126, 127]. In 2002, more general linear Regge trajectories were proposed in evaluating the semiclassical expansion of an effective string theory about a classical rotating string solution for long distance QCD, where the linear relationship between  $n$  and  $M^2$  appeared[128]. In 2011, Ebert *et al.* constructed the heavy baryon Regge trajectories in both the  $(J, M^2)$  and the  $(n, M^2)$  planes [58].

In this subsection, we investigate the Regge trajectories in the  $(J, M^2)$  plane based on our calculated mass spectra of the strange single heavy baryons. The states in a baryon family can be classified

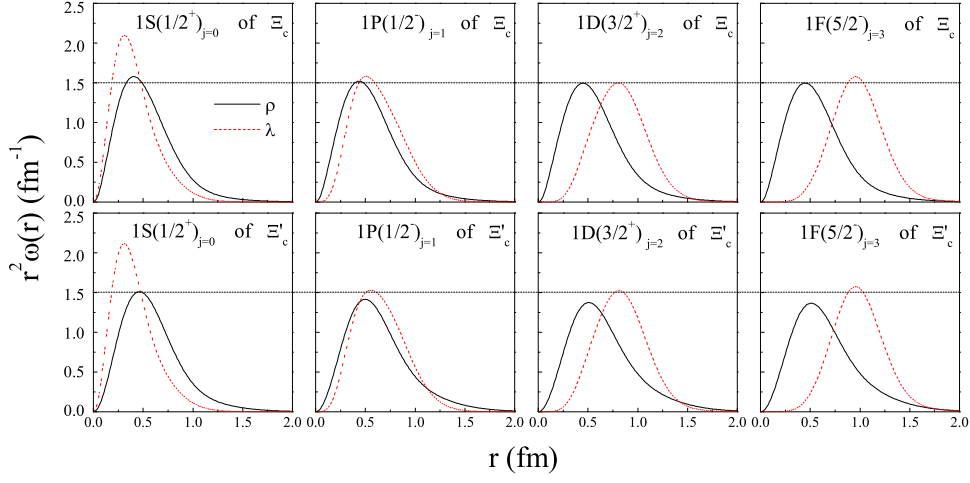


FIG. 5: (Color online)Radial probability density distributions for some  $1L$  states in the  $\Xi_c$  and  $\Xi'_c$  families. The black line denotes the probability density with  $r_\rho$ , and the dash line denotes the one with  $r_\lambda$ .

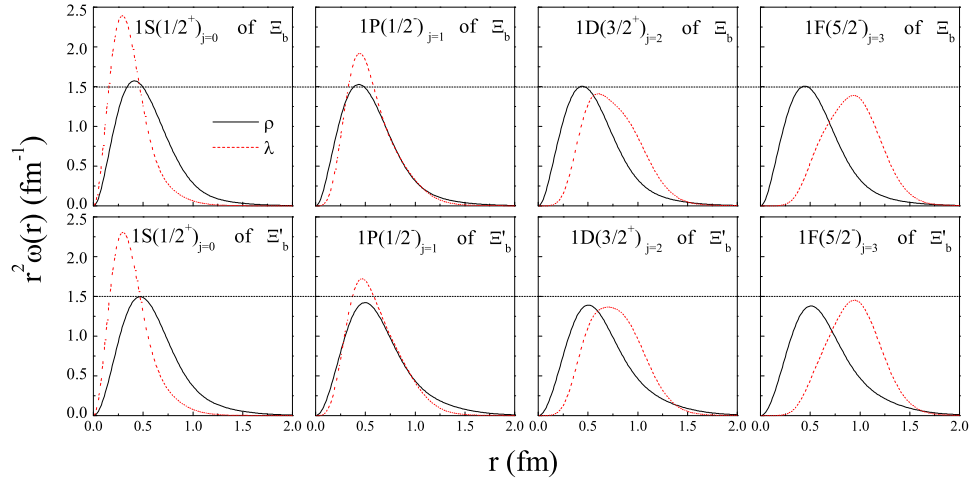


FIG. 6: (Color online)Same as Fig.5, but for the  $\Xi_b$  and  $\Xi'_b$  families.

according to the following parities and angular momenta: (1) Natural  $P = (-1)^{J+1/2}$  and unnatural  $P = (-1)^{J-1/2}$  parities (written in short as  $NP$  and  $UP$ , respectively)[129]; (2)  $J = j + 1/2$  and  $J = j - 1/2$  (written in short as  $NJ$  and  $UJ$ ). Thus, the states in the  $\Xi_c$  or  $\Xi_b$  family are divided into two groups, and the states in the  $\Xi'_c$  or  $\Xi'_b$  family are divided into six groups. In this paper, we

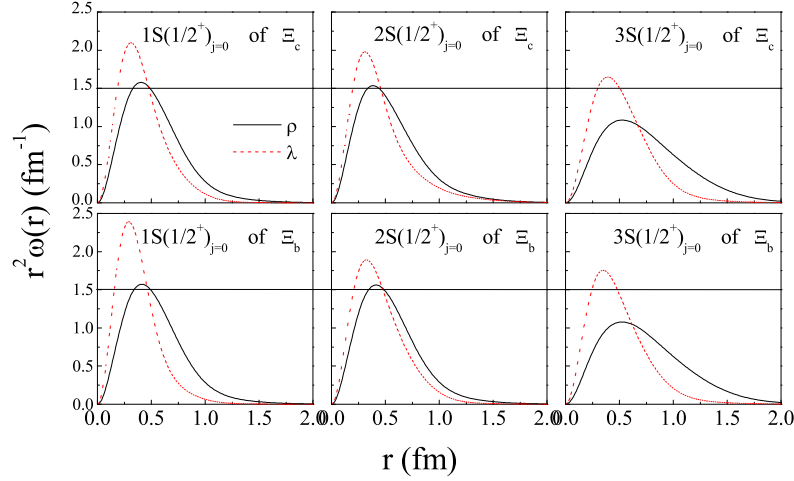


FIG. 7: (Color online) Radial probability density distributions for some  $nS$  states in the  $\Xi_c$  and  $\Xi_b$  families.

use the following definition for the  $(J, M^2)$  Regge trajectories,

$$M^2 = \alpha J + \beta, \quad (32)$$

where  $\alpha$  and  $\beta$  are the slope and intercept. In Figs. 7 and 8, we plot the Regge trajectories in the  $(J, M^2)$  plane with our calculated mass spectra. The three lines in each figure correspond to the radial quantum number  $n = 1, 2, 3$ , respectively. The fitted slopes and intercepts of the Regge trajectories are given in Tables VII and VIII.

It is shown that the linear trajectories appear clearly in the  $(J, M^2)$  plane. All the data points fall on the trajectory lines. This indicates that the Regge trajectory has a strong universality and our theoretical calculations are reliable. These trajectories are almost parallel, but not equidistant, which is an apparent difference between our mass spectra and those in reference [58].

In this paper, we do not show the Regge trajectories in the  $(n, M^2)$  plane. In fact, the linear trajectories in the  $(n, M^2)$  plane can not be constructed from our predicted masses. As will be mentioned in subsection 3.5, the observation of heavy baryons in forthcoming experiments is difficult to touch the  $3S$  sub shell. So it is difficult to check the  $(n, M^2)$  Regge trajectories, and we could not judge whether single heavy baryons are a three-quark system or a quark-diquark system as well.

### 3.4 Preliminary assignment to some observed heavy baryons

We first pay attention to the well determined  $\Xi_c$  ( $\Xi_c'$ ) baryons in the PDG. As shown in Table I,  $\Xi_c^+$  and  $\Xi_c^0$  as an isospin doublet, can be assigned to be the  $\Xi_c$   $1S(\frac{1}{2}^+)$  state. Similarly,  $\Xi_c'^{+,0}$  are

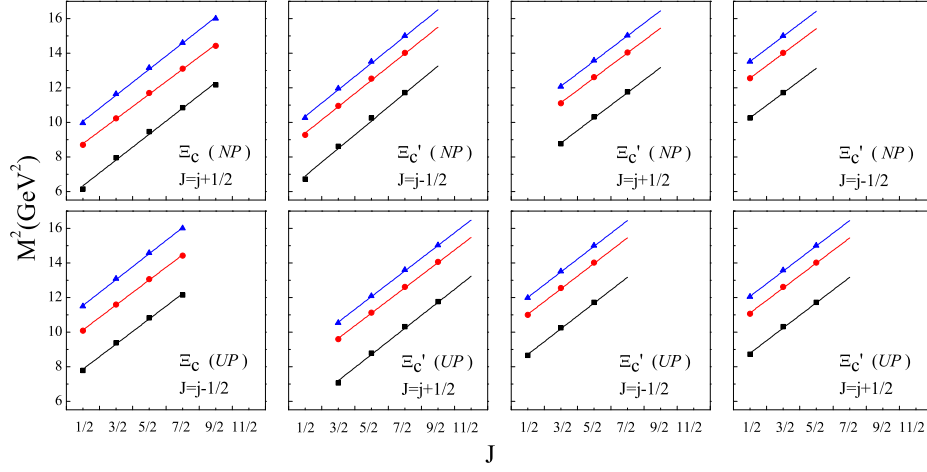


FIG. 8: (Color online)  $(J, M^2)$  Regge trajectories for the  $\Xi_c$  ( $\Xi'_c$ ) families and  $M^2$  is in  $\text{GeV}^2$ .

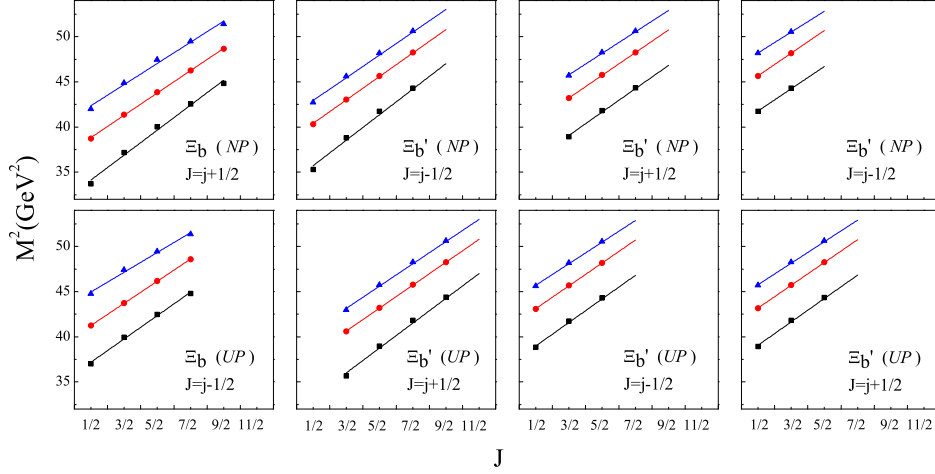


FIG. 9: (Color online)  $(J, M^2)$  Regge trajectories for the  $\Xi_b$  ( $\Xi'_b$ ) families and  $M^2$  is in  $\text{GeV}^2$ .

likely to be the  $1S(\frac{1}{2}^+)$  state of  $\Xi'_c$  (see Table II). In the same way,  $\Xi_c(2645)^{+,0}$  should correspond to the  $1S(\frac{3}{2}^+)$  state of  $\Xi'_c$  in Table II.  $\Xi_c(2790)^{+,0}$  and  $\Xi_c(2815)^{+,0}$  are relatively well-determined  $P$ -wave  $\Xi_c$  baryons with quantum numbers  $J^P = \frac{1}{2}^-$  and  $\frac{3}{2}^-$ , respectively, as shown in Table I. By the assignment of these charm-strange baryons, we find the measured masses can be well reproduced in our calculations and the deviation is usually less than 14 MeV. Additionally, it needs to be noted that  $\Xi_c(2645)$  should be a member of  $\Xi'_c$  family. So it ought to be labelled with  $\Xi'_c(2645)$ .

$\Xi_c(2970)$ , earlier known as  $\Xi_c(2980)$ , was first observed by the Belle [4] in 2006. Now the quantum numbers of  $\Xi_c(2970)$  are determined as  $\frac{1}{2}^+$  in the latest PDG. In our calculations, the only candidate with the same  $J^P$  for that baryon, is the  $2S(\frac{1}{2}^+)$  of  $\Xi_c$  as shown in Tables I. And the predicted mass is smaller 15 MeV than the experimental data. At last,  $\Xi_c(3055)$  and  $\Xi_c(3080)$  were observed by the BABAR [5] and the Belle [4, 11, 16]. As shown in the PDG, the spin and parity values of them have not yet been clear so far. According to the measured masses of  $\Xi_c(3055)$  and  $\Xi_c(3080)$ , they are likely to be the  $1D$  doublet  $(\frac{3}{2}^+, \frac{5}{2}^+)$  of  $\Xi_c$  in Table I or the  $2S$  doublet  $(\frac{1}{2}^+, \frac{3}{2}^+)$  of  $\Xi'_c$  in Table II. Considering the system with a smaller root mean square radius (especially for  $\langle r_\lambda^2 \rangle^{1/2}$ ) is more stable, the  $2S$  doublet states should then be the ideal candidates, because their  $\langle r_\lambda^2 \rangle^{1/2}$  values are smaller than those of the  $1D$  doublet states.

Outside of the PDG data, the Belle and the LHCb observed four charm-strange baryons, namely  $\Xi_c(2930)$  [13],  $\Xi_c(2923)$ ,  $\Xi_c(2939)$ , and  $\Xi_c(2964)$  [14], whose masses are very close to each other. By the predicted masses in Tables I and II, the above four baryons can be assigned to be the first orbital ( $1P$ ) excitation of  $\Xi'_c$  or the first radial ( $2S$ ) excitation of  $\Xi_c$ . At present, we can not determine their quantum numbers accurately.

The  $\Xi_c(3123)$  was observed by the BABAR Collaboration [5]. However, it has not yet appeared in the PDG [30] so far. In our calculations, the predicted masses of the  $\Xi_c 3S(\frac{1}{2}^+)$  and  $\Xi'_c 2S(\frac{3}{2}^+)$  are 3155 MeV and 3095 MeV, respectively, which are relatively closer to the measured value of the  $\Xi_c(3123)$  than those of other states. The  $\Xi'_c 2S(\frac{3}{2}^+)$  has been considered as the candidate of the  $\Xi_c(3080)$ . Then, the  $\Xi_c(3123)$  is likely to be the  $\Xi_c 3S(\frac{1}{2}^+)$  state.

The calculated mass spectra of  $\Xi_b$  and  $\Xi'_b$  families are listed in Tables IV-VI where a total of six bottom-strange baryons with determined quantum numbers in the PDG have been assigned to the possible states. The mass and  $J^P$  values of  $\Xi_b^{-,0}$  are consistent with those of the  $\Xi_b 1S(\frac{1}{2}^+)$  state as shown in Table IV. Similarly,  $\Xi'_b(5935)^-$  should correspond to the  $\Xi'_b 1S(\frac{1}{2}^+)$  state in Table V.  $\Xi_b(5945)^0$  and its isospin partner  $\Xi_b(5955)^-$  can be assigned to the  $\Xi'_b 1S(\frac{3}{2}^+)$  state in Table V. In 2021, AMS collaboration determined the  $\Xi_b(6100)$  with the quantum numbers  $J^P = \frac{3}{2}^-$  by measuring the typical decay chain of  $\Xi_b(6100)^- \rightarrow \Xi_b^{*0} \pi^- \rightarrow \Xi_b^- \pi^+ \pi^-$  [26]. Very recently, the values of  $J^P = \frac{3}{2}^-$  of  $\Xi_b(6100)$  were written into the PDG data. Table IV shows the mass of the  $\Xi_b(6100)$  is very close to that of the  $\Xi_b 1P(\frac{3}{2}^-)$  state. So, the  $\Xi_b(6100)$  is most likely to be the  $1P(\frac{3}{2}^-)$  state of  $\Xi_b$ . From Tables IV and V, we find the experimental data can be well reproduced by our theoretical calculations. In addition, it should be pointed out  $\Xi_b(5945)^0$  and  $\Xi_b(5955)^-$  belong to the  $\Xi'_b$  family in our calculations. So, they ought to be labelled with  $\Xi'_b(5945)^0$  and  $\Xi'_b(5955)^-$ .

The last two  $\Xi_b$  baryons in the PDG,  $\Xi_b(6227)^-$  and  $\Xi_b(6227)^0$ , were reported by the LHCb Collaboration in 2018 [25]. But their spin and parity values are still not confirmed. In Tables IV and V, there are six states (one  $2S$  state of  $\Xi_b$  and five  $1P$  states of  $\Xi'_b$ ) whose masses range from 6224 MeV

to 6243 MeV. Each of them could be considered as a possible assignment to the  $\Xi_b(6227)$ .

In 2021, two bottom-strange baryons  $\Xi_b(6327)$  and  $\Xi_b(6333)$  were reported by the LHCb Collaboration. Very recently, the LHCb implied in experiment that they should belong to the  $\Xi_b$   $1D(\frac{3}{2}^+, \frac{5}{2}^+)$  doublet [27]. In Table IV, one can see the predicted masses of the  $1D$  doublet  $(\frac{3}{2}^+, \frac{5}{2}^+)$  of  $\Xi_b$  indeed match with the experimental data of the  $\Xi_b(6327)$  and  $\Xi_b(6333)$ .

From the above analyses and discussion, we find the masses from the experimentally determined  $\Xi_Q$  baryons can be reproduced nicely in this work. The accuracy of the predicted masses is impressive. Therefore, the calculated mass spectra of the  $\Xi_Q$  families can be used as important and reliable reference data. Nevertheless, one can see only the mass spectra could not give accurate predictions for those baryons as mentioned above and more theoretical studies need to be done, such as their strong decay properties which will be our next mission.

### 3.5 Shell structure of the mass spectra

To get a clear outline of the baryon spectra, the mass spectra of the  $\Xi_c$  ( $\Xi'_c$ ) and  $\Xi_b$  ( $\Xi'_b$ ) baryons are mapped to the planes with column and row indices  $nL$  and  $J$  as shown in Tables IX and X, respectively. In these tables, those masses which have been experimentally well established are marked in boldface. Some observed baryons are also labeled in brackets following their possible masses. Each table includes two families, i.e., the  $6_F$  family (on the top half) and the  $\bar{3}_F$  family (on the bottom half). According to the discussion of the root mean square radius in subsection 3.2, only the physically allowed states are collected in these tables. Here we only list the states with their root mean square radii less than 1 fm. And the corresponding values of  $\langle r_\rho^2 \rangle^{1/2}$  and  $\langle r_\lambda^2 \rangle^{1/2}$  are listed in the last two columns of each table. The masses are arranged in ascending order from smallest to largest. It is shown the mass distribution presents an obvious shell structure, which is analogous to the energy level structure in a nucleus.

From these two tables, we could get a bird's-eye view of the mass spectra. Firstly, the baryon spectra of the  $\Xi_c$  ( $\Xi'_c$ ) and  $\Xi_b$  ( $\Xi'_b$ ) almost have the same shell structure. Secondly, the baryons with lighter masses were discovered earlier in experiment. Thirdly, the calculated masses for the  $2S$  states of  $\bar{3}_F$  family and the  $1P$  states of  $6_F$  family are very close to each other. This makes them hard to be identified in both experiment and theory.

At last, the states which are possibly observed in experiment can be predicted by this method. When the root mean square radius is greater than 0.9 fm, the resonance state might become even more unstable. So, the  $3S$ ,  $2P$  and  $1F$  states of  $\Xi_c$  are difficult to be observed experimentally as shown in Table IX. The same is true for the  $3S$  and  $2P$  states of  $\Xi'_c$ . Therefore, the new charm-strange baryons which are most likely to be found in experiment might belong to the  $1D$  states of



$\Xi'_c$  with the predicted masses ranging from 3201 MeV to 3213 MeV. Additionally, the  $1D$  doublet states of  $\Xi_c$  should have been observed in experiment, and the masses range from 3063 MeV to 3076 MeV. For the  $\Xi_b$  ( $\Xi'_b$ ) families, there are more physically allowed resonance states than those of  $\Xi_c$  ( $\Xi'_c$ ) families as shown in Table X. The  $\Xi_b$   $1P(\frac{1}{2}^-)$  is very likely to be found first in experiment and the predicted mass is 6084 MeV.

#### IV. Conclusions

Motivated by the experimental development of singly heavy baryons and the theoretical work of Ebert *et al.*, we investigate the strange single heavy baryon spectra in a three-quark system, where the baryon model developed by Capstick and Isgur and the ISG method are employed. Considering the feature that the  $\lambda$ -mode appears lower in energy for definite states  $nL(J^P)$ , we only focus on the  $\lambda$ -mode and ignore the mixing among the different modes, which is certainly an approximation, and obtain the complete mass spectra of the  $\Xi_c$ ,  $\Xi'_c$ ,  $\Xi_b$  and  $\Xi'_b$  families. For the well established baryons, our predicted masses can nicely reproduce the experimental data, which indicates that our approximation is rather reasonable.

We also investigate the root mean square radii and the radial probability density distributions of the strange single heavy baryons, from which we can predict the upper limit of the mass spectrum and constrain the number of members for each heavy baryon family.

Based on the predicted mass spectra, we put forward a more detailed classification method to construct the Regge trajectories in the  $(J, M^2)$  plane. Nevertheless, we can not currently construct the linear trajectories in the  $(n, M^2)$  plane, which is an apparent difference between our mass spectra and those in the relativistic quark-diquark picture [58].

For some recently observed baryons, we preliminarily assign them reasonable positions in the obtained mass spectra. At last, the mass spectral structure of the  $\Xi_c$  ( $\Xi'_c$ ) and  $\Xi_b$  ( $\Xi'_b$ ) families is presented, from which we could get a bird's-eye view of the mass spectra and easily foresee where the experiment is going. Then, we predict several resonance states which might be observed in the forthcoming experiments.

#### Acknowledgements

One of the authors Zhen-Yu Li thanks Wen-Chao Dong for providing valuable references, useful discussions and kind help in the program design. And Li is also grateful to Professor Xian-Jian Shi for his support and encouragement. This work could not have been done without the joint efforts of all members of the phenomenological QCD theory group in North China Electric Power University. This

research is supported by the Science and Technology Talent Project of Education Bureau of Guizhou Province, China (QJHKY [2018]058)), the National Natural Science Foundation of China (Grant No. 11675265), the Continuous Basic Scientific Research Project (Grant No. WDJC-2019-13), and the Leading Innovation Project (Grant No. LC 192209000701).

- 
- [1] P. Avery, et al. [CLEO Collaboration], Phys. Rev. Lett. 75, 4364-4368 (1995), arXiv:hep-ex/9508010.
  - [2] R. Mizuk, et al. [Belle Collaboration], Phys. Rev. Lett. 94, 122002 (2005), arXiv:hep-ex/0412069.
  - [3] B. Aubert, et al. [BaBar Collaboration], arXiv:hep-ex/0607042.
  - [4] R. Chistov, et al. [Belle Collaboration], Phys. Rev. Lett. 97, 162001 (2006), arXiv:hep-ex/0606051.
  - [5] B. Aubert, et al. [BABAR Collaboration], Phys. Rev. D 77, 012002, (2008), arXiv:0710.5763 [hep-ex]
  - [6] B. Aubert, et al. [BaBar Collaboration], Phys. Rev. Lett. 97, 232001 (2006), arXiv:hep-ex/0608055.
  - [7] B. Aubert, et al. [BaBar Collaboration], Phys. Rev. Lett. 98, 012001 (2007), arXiv:hep-ex/0603052.
  - [8] K. Abe, et al. [Belle Collaboration], Phys. Rev. Lett. 98, 262001 (2007), arXiv:hep-ex/0608043.
  - [9] B. Aubert, et al. [BaBar Collaboration], Phys. Rev. D 77, 031101 (2008).
  - [10] T. Lesiak, et al. [Belle Collaboration], Phys. Lett. B 665, 9 (2008), arXiv:0802.3968[hep-ex].
  - [11] Y. Kato, et al. [Belle Collaboration], Phys. Rev. D 89, 052003 (2014), arXiv:1312.1026 [hep-ex].
  - [12] E. Solovieva, et al., Phys. Lett. B 672, 1 (2009), arXiv:0808.3677 [hep-ex].
  - [13] Y. B. Li, et al. [Belle Collaboration], Eur. Phys. J. C 78, 928 (2018), arXiv:1806.09182 [hep-ex].
  - [14] R. Aaij, et al. [LHCb collaboration], Phys. Rev. Lett. 124, 222001 (2020), arXiv:2003.13649 [hep-ex].
  - [15] T. J. Moon, et al. [Belle Collaboration], Phys. Rev. D 103, 111101 (2021), arXiv:2007.14700 [hep-ex].
  - [16] Y. Kato, et al. [Belle Collaboration], Phys. Rev. D 94, 032002 (2016), arXiv:1605.09103 [hep-ex].
  - [17] P. Abreu, et al. [DELPHI Collaboration], Z. Phys. C 68, 541 (1995).
  - [18] V. Abazov, et al. [D0 Collaboration], Phys. Rev. Lett. 99, 052001 (2007), arXiv:0706.1690 [hep-ex].
  - [19] T. Aaltonen, et al. [CDF Collaboration], Phys. Rev. Lett. 99, 052002 (2007), arXiv:0707.0589 [hep-ex].
  - [20] T. Aaltonen [CDF Collaboration], Phys. Rev. Lett. 107, 102001 (2011), arXiv:1107.4015 [hep-ex].
  - [21] CMS Collaboration, Phys. Rev. Lett 108, 252002 (2012), arXiv:1204.5955 [hep-ex].
  - [22] R. Aaij, et al. [LHCb Collaboration], Phys. Rev. Lett. 114, 062004 (2015).
  - [23] R. Aaij, et al. [LHCb Collaboration], J. High Energy Phys. 05, 161 (2016).
  - [24] R. Aaij, et al. [LHCb Collaboration], Phys. Rev. Lett. 121, 072002 (2018), arXiv:1805.09418 [hep-ex].
  - [25] R. Aaij, et al. [LHCb Collaboration], Phys. Rev. Lett. 121, 072002 (2018).
  - [26] A. M. Sirunyan, et al. [CMS Collaboration], Phys. Rev. Lett. 126, 252003 (2021).
  - [27] R. Aaij, et al. [LHCb collaboration], Phys. Rev. Lett. 128, 162001 (2022), arXiv:2110.04497 [hep-ex].
  - [28] R. Aaij, et al. [LHCb Collaboration], Phys. Rev. Lett. 122, 012001 (2019), arXiv:1809.07752.
  - [29] R. Aaij, et al. [LHCb Collaboration], Phys. Rev. Lett. 123, 152001 (2019).
  - [30] P. A. Zyla, et al. [Particle Data Group], Prog. Theor. Exp. Phys. 083C01 (2020).
  - [31] R.Chistov, et al. [Belle Collaboration], Phys. Rev. Lett. 97, 162001 (2006).
  - [32] L. H. Liu, L. Y. Xiao, and X. H. Zhong, Phys. Rev. D 86, 034024 (2012), arXiv:1205.2943 [hep-ph].

- [33] D. D. Ye, Z. Zhao and A. Zhang, Phys. Rev. D 96, 114009 (2017), arXiv:1709.00689 [hep-ph].
- [34] Z. Zhao, D. D. Ye and A. Zhang, Phys. Rev. D 94, 114020 (2016).
- [35] Y. X. Yao, K. L. Wang and X. H. Zhong, Phys. Rev. D 98 076015 (2018), arXiv:1803.00364.
- [36] H. X. Chen, Q. Mao, A. Hosaka et al., Phys. Rev. D 94, 114016 (2016), arXiv:1611.02677v2 [hep-ph].
- [37] D. D. Ye, Z. Zhao and A. Zhang, Phys. Rev. D 96, 114003 (2017), arXiv:1710.10165 [hep-ph].
- [38] Z. G. Wang, Nucl. Phys. B 926, 467 (2018), arXiv:1705.07745 [hep-ph].
- [39] H. X. Chen and Q. Mao, Atsushi Hosaka et al. Phys. Rev. D 94, 114016 (2016), arXiv:1611.02677 [hep-ph].
- [40] B. Roelof, G. T. Hugo, G. Alessandro, et al., arXiv:2010.12437 [hep-ph].
- [41] K. L. Wang, Y. X. Yao, X. H. Zhong, et al., Phys. Rev. D 96, 116016 (2017). arXiv: hep-ph/1709.04268.
- [42] B. Chen, K. W. Wei and A. Zhang, Eur. Phys. J. A 51, 82 (2015), arXiv: hep-ph/1406.6561v4.
- [43] B. Chen, X. Liu and A. Zhang, Phys. Rev. D 95, 074022 (2017).
- [44] Z. G. Wang and H. J. Wang, Chin. Phys. C 45 013109 (2021) arXiv:2006.16776 [hep-ph].
- [45] J. Nieves, R. Pavao and L. Tolos, Eur. Phys. J. C 80, 22 (2020), arXiv:1911.06089 [hep-ph].
- [46] K. Gandhi and A. Kumar Rai, Eur. Phys. J. Plus 135, 213 (2020), arXiv:1911.11039 [hep-ph].
- [47] Z. Zhao, Phys. Rev. D 102, 096021 (2020), arXiv:2008.00630 [hep-ph].
- [48] B. Chen, K. W. Wei and A. Zhang, Eur. Phys. J. A 51, 82 (2015), arXiv:1406.6561 [hep-ph].
- [49] K. L. Wang, Q. F. Lü, and X. H. Zhong, Phys. Rev. D 99, 014011 (2019).
- [50] Y. Huang, C. J. Xiao, L. S. Geng et al., Phys. Rev. D 99, 014008 (2019).
- [51] B. Chen, K. W. Wei, X. Liu et al., Phys. Rev. D 98, 031502 (2018), arXiv:1805.10826 [hep-ph].
- [52] H. J. Wang, Z. Y. Di and Z. G. Wang, Int. J. Theor. Phys. 59(10): 3124-3133,(2020).
- [53] K. Azizi, Y. Sarac and H. Sundu, Journal of High Energy Physics 2021, 244 (2021), arXiv:2012.01086 [hep-ph].
- [54] G. L. Yu, Z. G. Wang and X. W. Wang, arXiv:2109.02217 [hep-ph].
- [55] H. M. Yang, H. X. Chen, E. L. Cui et al., arXiv:2205.07224 [hep-ph].
- [56] W. J. Wang, Y. H. Zhou, L. Y. Xiao, et al., Phys. Rev. D 105, 074008 (2022), arXiv:2202.05426 [hep-ph].
- [57] D. Ebert, R. N. Faustov and V. O. Galkin, Phys. Lett. B 659, 612 (2008), arXiv:0705.2957v2.
- [58] D. Ebert, R. N. Faustov and V. O. Galkin, Phys. Rev. D 84, 014025 (2011),
- [59] R. N. Faustov and V. O. Galkin, Phys. Rev. D 105, 014013 (2022), arXiv: hep-ph/2111.07702v1.
- [60] H. Mutuk, Eur. Phys. J. Plus 137:10 (2022), arXiv: hep-ph/2112.06205v1.
- [61] S. Capstick and N. Isgur, Phys. Rev. D 34, 2809 (1986).
- [62] G. L. Yu, Z. Y. Li, Z. G. Wang, et al., arXiv:2206.08128 [hep-ph]
- [63] T. Yoshida, E. Hiyama, A. Hosaka, et al., Phys. Rev. D 92, 114029 (2015). arXiv: hep-ph/1510.01067.
- [64] G. Yang, J. Ping, and J. Segovia, Few Body Syst. 59, 113 (2018). arXiv:1709.09315 [hep-ph].
- [65] G. Yang, J. Ping, P. G. Ortega, et al., Chinese Phys. C 44, 023102 (2020). arXiv:1904.10166 [hep-ph].
- [66] J. Segovia, D. R. Entem, F. Fernandez, et al., Int. J. Mod. Phys. E 22, 1330026 (2013). arXiv:1309.6926.
- [67] M. Q. Huang, Y. B. Dai and C. S. Huang, Phys. Rev. D 52, 3986 (1995); 55, 7317(E) (1997).
- [68] M. C. Banuls, A. Pich and I. Scimemi, Phys. Rev. D 61, 094009 (2000).
- [69] H. Y. Cheng and C. K. Chua, Phys. Rev. D 75, 014006 (2007).
- [70] N. Jiang, X. L. Chen and S. L. Zhu, Phys. Rev. D 92, 054017 (2015).

- [71] H. Y. Cheng and C. K. Chua, Phys. Rev. D 92, 074014 (2015).
- [72] X. H. Guo, K. W. Wei and X. H. Wu, Phys. Rev. D 77, 036003 (2008).
- [73] G. L. Yu, Z. G. Wang and Z. Y. Li, Chinese Physics C 39, 6, 063101 (2015), arXiv: hep-ph/1402.5955.
- [74] H. Z. He, W. Liang and Q. F. Lü, Phys. Rev. D 105, 014010 (2022), arXiv: hep-ph/2106.11045v2.
- [75] C. Chen, X. L. Chen, X. Liu et al., Phys. Rev. D 75, 094017 (2007).
- [76] P. Yang, J. J. Guo and A. Zhang, Phys. Rev. D 99, 034018 (2019), arXiv:1810.06947 [hep-ph].
- [77] J. J. Guo, P. Yang, and A. Zhang, Phys. Rev. D 100, 014001 (2019), arXiv:1902.07488 [hep-ph].
- [78] W. Liang, Q. F. Lü and X. H. Zhong, Phys. Rev. D 100, 054013 (2019).
- [79] Q. F. Lü and X. H. Zhong, Phys. Rev. D 101, 014017 (2020).
- [80] H. Z. He, W. Liang, Q. F. Lü et al., Sci. China Phys. Mech. Astron. 64, 261012(2021).
- [81] M. Padmanath, R. G. Edwards, N. Mathur et al., arXiv:1311.4806.
- [82] H. Bahtiyar, K. U. Can, G. Erkol et al., Phys. Lett. B 747, 281 (2015).
- [83] P. Perez-Rubio, S. Collins and G. S. Bali, Phys. Rev. D 92, 034504 (2015).
- [84] H. Bahtiyar, K. U. Can, G. Erkol et al., Phys. Lett. B 772, 121 (2017).
- [85] C. K. Chow, Phys. Rev. D 54, 3374 (1996).
- [86] S. L. Zhu and Y. B. Dai, Phys. Rev. D 59, 114015 (1999).
- [87] S. S. Agaev, K. Azizi and H. Sundu, Phys. Rev. D 96, 094011 (2017).
- [88] H. X. Chen, Q. Mao, W. Chen et al., Phys. Rev. D 95, 094008 (2017).
- [89] Z. G. Wang, Phys. Rev. D 81, 036002 (2010).
- [90] Z. G. Wang, Eur. Phys. J. A 44, 105 (2010).
- [91] T. M. Aliev, K. Azizi and H. Sundu, Eur. Phys. J. C 75, 14 (2015).
- [92] T. M. Aliev, K. Azizi and A. Ozipineci, Phys. Rev. D 79, 056005 (2009).
- [93] T. M. Aliev, T. Barakat and M. Savc, Phys. Rev. D 93, 056007 (2016).
- [94] T. M. Aliev, K. Azizi and M. Savci, Phys. Lett. B 696, 220(2011).
- [95] T. M. Aliev, K. Azizi, Y. Sarac et al., Phys. Rev. D 99, 094003 (2019).
- [96] S. L. Zhu, Phys. Rev. D 61, 114019 (2000).
- [97] Z. G. Wang, Eur. Phys. J. A 47, 81 (2011).
- [98] Q. Mao, H. X. Chen, W. Chen et al., Phys. Rev. D 92, 114007 (2015), arXiv:1510.05267 [hep-ph].
- [99] H. X. Chen, Q. Mao, A. Hosaka et al., Phys. Rev. D 94, 114016 (2016).
- [100] Q. Mao, H. X. Chen, A. Hosaka et al., Phys. Rev. D 96, 074021 (2017).
- [101] T. M. Aliev, K. Azizi, Y. Sarac et al., Phys. Rev. D 98, 094014 (2018).
- [102] E. L. Cui, H. M. Yang, H. X. Chen et al., Phys. Rev. D 99, 094021 (2019).
- [103] K. Azizi, Y. Sarac and H. Sundu, Phys. Rev. D 101, 074026 (2020).
- [104] K. Azizi, Y. Sarac and H. Sundu, Phys. Rev. D 102, 034007 (2020).
- [105] Z. G. Wang, Eur. Phys. J. C, 75(8), 359 (2015).
- [106] S. Godfrey and N. Isgur, Phys. Rev. D 32, 189 (1985).
- [107] E. Hiyama, Y. Kino and M. Kamimura, Prog. Part. Nucl. Phys. 51, 223 (2003).
- [108] Q. F. Lü, D. Y. Chen and Y. B. Dong, Phys. Rev. D 102, 034012 (2020).
- [109] Q. F. Lü, D. Y. Chen and Y. B. Dong, Eur. Phys. J. C 80, 871 (2020).
- [110] Q. F. Lü, D. Y. Chen and Y. B. Dong, Phys. Rev. D 102, 074021 (2020).

- [111] E. Hiyama, A. Hosaka, M. Oka et al., Phys. Rev. C 98, 045208 (2018), arXiv:1803.11369v1 [nucl-th].
- [112] H. X. Chen, W. Chen, X. Liu, et al. Physics Reports 639,1-121(2016), arXiv:1601.02092 [hep-ph].
- [113] F. K. Guo, C. Hanhart, U. G. Meißner, et al., Rev. Mod. Phys. 90,015004(2018), arXiv:1705.00141 [hep-ph].
- [114] R. Aaij, et al.,[LHCb collaboration], Phys. Rev. Lett. 122,222001(2019), arXiv:1904.03947 [hep-ex].
- [115] X. K. Dong, F. K. Guo, B. S. Zou,Commun. Theor. Phys. 73(2021)125201, arXiv:2108.02673 [hep-ph].
- [116] T. Ji, X. K. Dong, F. K. Guo, et al.,Phys. Rev. Lett. 129,102002(2022), arXiv:2205.10994 [hep-ph].
- [117] C. Q. Pang, J. Z. Wang, X. Liu et al., Eur. Phys. J. C 77, 861 (2017).
- [118] H. Georgi, Physics Letters B 240, 447–450, (1990).
- [119] B. Chen, S. Q. Luo, X. Liu et al., Phys. Rev. D 100, 094032 (2019), arXiv:1910.03318.
- [120] H. X. Chen, W. Chen, X. Liu et al., Rept. Prog. Phys. 80, 7, 076201 (2017), arXiv:1609.08928,
- [121] H. Garcilazo, J. Vijande and A. Valcarce, J. phys. G 34, 961(2007).
- [122] S. Migura, D. Merten, B. Metsch et al., Eur. Phys. J. A 28, 41 (2006).
- [123] A. Martin, Z. Phys. C 32, 359 (1986).
- [124] T. Regge, Nuovo Cim. 14, 951 (1959).
- [125] T. Regge, Nuovo Cim. 18, 947–956 (1960).
- [126] G. F. Chew and S. C. Frautschi, Phys. Rev. Lett. 7, 394–397 (1961) .
- [127] G. F. Chew and S. C. Frautschi, Phys. Rev. Lett. 8, 41–44 (1962).
- [128] M. Baker and R. Steinke, Phys. Rev. D 65, 094042 (2002).
- [129] P. D. B. Collins, An Introduction to Regge Theory and High Energy Physics (Cambridge University Press),Cambridge, England, 1977.

## Appendix

TABLE I: The root mean square radius (fm) and the mass spectrum (MeV) of the  $\Xi_c$  family.

$l_\rho \ l_\lambda \ L \ s \ j$	$nL(J^P)$	$\langle r_\rho^2 \rangle^{1/2}$	$\langle r_\lambda^2 \rangle^{1/2}$	mass	exp.[30]	[58]
0 0 0 0 0	$1S(\frac{1}{2}^+)$	0.512	0.437	2479	$\Xi_c^+ 2467.71(0.23)$ $\Xi_c^0 2470.44(0.28)$	2476
	$2S(\frac{1}{2}^+)$	0.645	0.768	2949	2970?	2959
	$3S(\frac{1}{2}^+)$	0.968	0.607	3155	3123?[5]	3323
	$4S(\frac{1}{2}^+)$	0.690	1.131	3318		3632
0 1 1 0 1	$1P(\frac{1}{2}^-)$	0.542	0.627	2789	2791.9(0.5) 2793.9(0.5)	2792
	$2P(\frac{1}{2}^-)$	0.615	0.948	3176		3179
	$3P(\frac{1}{2}^-)$	1.038	0.763	3390		3500
	$4P(\frac{1}{2}^-)$	0.655	1.285	3492		3785
0 1 1 0 1	$1P(\frac{3}{2}^-)$	0.550	0.654	2819	2816.51(0.25) 2819.79(0.30)	2819
	$2P(\frac{3}{2}^-)$	0.613	0.977	3199		3201
	$3P(\frac{3}{2}^-)$	1.053	0.779	3412		3519
	$4P(\frac{3}{2}^-)$	0.645	1.278	3508		3804
0 2 2 0 2	$1D(\frac{3}{2}^+)$	0.561	0.825	3063	3055?	3059
	$2D(\frac{3}{2}^+)$	0.601	1.161	3406		3388
	$3D(\frac{3}{2}^+)$	1.084	0.936	3617		3678
	$4D(\frac{3}{2}^+)$	0.627	1.349	3676		3945
0 2 2 0 2	$1D(\frac{5}{2}^+)$	0.565	0.843	3076	3080?	3076
	$2D(\frac{5}{2}^+)$	0.604	1.190	3419		3407
	$3D(\frac{5}{2}^+)$	1.092	0.945	3627		3699
	$4D(\frac{5}{2}^+)$	0.618	1.328	3688		3965
0 3 3 0 3	$1F(\frac{5}{2}^-)$	0.567	0.998	3289		3278
	$2F(\frac{5}{2}^-)$	0.604	1.413	3613		3572
	$3F(\frac{5}{2}^-)$	1.103	1.087	3817		3845
	$4F(\frac{5}{2}^-)$	0.602	1.314	3861		4098
0 3 3 0 3	$1F(\frac{7}{2}^-)$	0.569	1.009	3294		3292
	$2F(\frac{7}{2}^-)$	0.607	1.439	3619		3592
	$3F(\frac{7}{2}^-)$	1.111	1.088	3821		3865
	$4F(\frac{7}{2}^-)$	0.589	1.290	3871		4120
0 4 4 0 4	$1G(\frac{7}{2}^+)$	0.566	1.147	3486		3469
	$2G(\frac{7}{2}^+)$	0.612	1.676	3798		3745
	$3G(\frac{7}{2}^+)$	1.121	1.205	4000		
	$4G(\frac{7}{2}^+)$	0.559	1.222	4054		
0 4 4 0 4	$1G(\frac{9}{2}^+)$	0.567	1.154	3487		3483
	$2G(\frac{9}{2}^+)$	0.613	1.692	3799		3763
	$3G(\frac{9}{2}^+)$	1.126	1.208	4001		
	$4G(\frac{9}{2}^+)$	0.551	1.202	4064		

TABLE II: The root mean square radius (fm) and the mass spectrum (MeV) of the  $\Xi'_c$  family (Part I).

$l_\rho \ l_\lambda \ L \ s \ j$	$nL(J^P)$	$\langle r_\rho^2 \rangle^{1/2}$	$\langle r_\lambda^2 \rangle^{1/2}$	mass	exp.[30]	[58]
0 0 0 1 1	$1S(\frac{1}{2}^+)$	0.590	0.431	2590	$\Xi'_c{}^+ \ 2578.2(0.5)$ $\Xi'_c{}^0 \ 2578.7(0.5)$	2579
	$2S(\frac{1}{2}^+)$	0.821	0.705	3046	3055?	2983
	$3S(\frac{1}{2}^+)$	0.918	0.671	3201		3377
	$4S(\frac{1}{2}^+)$	0.897	1.053	3425		3695
0 0 0 1 1	$1S(\frac{3}{2}^+)$	0.611	0.476	2658	2645.10(0.30) 2646.16(0.25)	2654
	$2S(\frac{3}{2}^+)$	0.801	0.763	3095	3080?	3026
	$3S(\frac{3}{2}^+)$	0.968	0.676	3244		3396
	$4S(\frac{3}{2}^+)$	0.850	1.095	3456		3709
0 1 1 1 0	$1P(\frac{1}{2}^-)$	0.649	0.671	2952		2936
	$2P(\frac{1}{2}^-)$	0.762	0.978	3326		3313
	$3P(\frac{1}{2}^-)$	1.055	0.811	3469		3630
	$4P(\frac{1}{2}^-)$	0.783	1.245	3636		3912
0 1 1 1 1	$1P(\frac{1}{2}^-)$	0.644	0.659	2941		2854
	$2P(\frac{1}{2}^-)$	0.763	0.962	3315		3267
	$3P(\frac{1}{2}^-)$	1.048	0.804	3460		3598
	$4P(\frac{1}{2}^-)$	0.788	1.248	3628		3887
0 1 1 1 1	$1P(\frac{3}{2}^-)$	0.651	0.677	2958		2935
	$2P(\frac{3}{2}^-)$	0.761	0.985	3331		3311
	$3P(\frac{3}{2}^-)$	1.059	0.814	3473		3628
	$4P(\frac{3}{2}^-)$	0.780	1.243	3640		3911
0 1 1 1 2	$1P(\frac{3}{2}^-)$	0.642	0.653	2934	2930?[13]	2912
	$2P(\frac{3}{2}^-)$	0.764	0.955	3310		3293
	$3P(\frac{3}{2}^-)$	1.043	0.801	3456		3613
	$4P(\frac{3}{2}^-)$	0.791	1.249	3624		3898
0 1 1 1 2	$1P(\frac{5}{2}^-)$	0.652	0.682	2964	2970?	2929
	$2P(\frac{5}{2}^-)$	0.761	0.993	3335		3303
	$3P(\frac{5}{2}^-)$	1.062	0.817	3477		3619
	$4P(\frac{5}{2}^-)$	0.778	1.241	3644		3902
0 2 2 1 1	$1D(\frac{1}{2}^+)$	0.668	0.851	3201		3163
	$2D(\frac{1}{2}^+)$	0.744	1.195	3541		3505
	$3D(\frac{1}{2}^+)$	1.104	0.955	3676		
	$4D(\frac{1}{2}^+)$	0.738	1.303	3816		
0 2 2 1 1	$1D(\frac{3}{2}^+)$	0.671	0.865	3211		3167
	$2D(\frac{3}{2}^+)$	0.745	1.219	3550		3506
	$3D(\frac{3}{2}^+)$	1.111	0.963	3684		
	$4D(\frac{3}{2}^+)$	0.734	1.285	3827		

TABLE III: The root mean square radius (fm) and the mass spectrum (MeV) of the  $\Xi'_c$  family (Part II).

$l_\rho \ l_\lambda \ L \ s \ j$	$nL(J^P)$	$\langle r_\rho^2 \rangle^{1/2}$	$\langle r_\lambda^2 \rangle^{1/2}$	mass	[58]
0 2 2 1 2	$1D(\frac{3}{2}^+)$	0.668	0.851	3201	3160
	$2D(\frac{3}{2}^+)$	0.744	1.195	3541	3497
	$3D(\frac{3}{2}^+)$	1.104	0.955	3676	
	$4D(\frac{3}{2}^+)$	0.738	1.303	3816	
0 2 2 1 2	$1D(\frac{5}{2}^+)$	0.671	0.865	3211	3166
	$2D(\frac{5}{2}^+)$	0.745	1.219	3551	3504
	$3D(\frac{5}{2}^+)$	1.111	0.963	3685	
	$4D(\frac{5}{2}^+)$	0.734	1.285	3828	
0 2 2 1 3	$1D(\frac{5}{2}^+)$	0.667	0.850	3200	3153
	$2D(\frac{5}{2}^+)$	0.744	1.193	3540	3493
	$3D(\frac{5}{2}^+)$	1.104	0.954	3676	
	$4D(\frac{5}{2}^+)$	0.738	1.304	3815	
0 2 2 1 3	$1D(\frac{7}{2}^+)$	0.672	0.868	3213	3147
	$2D(\frac{7}{2}^+)$	0.746	1.224	3552	3486
	$3D(\frac{7}{2}^+)$	1.112	0.965	3686	
	$4D(\frac{7}{2}^+)$	0.733	1.281	3829	
0 3 3 1 2	$1F(\frac{3}{2}^-)$	0.676	1.022	3424	3418
	$2F(\frac{3}{2}^-)$	0.742	1.454	3744	
	$3F(\frac{3}{2}^-)$	1.136	1.096	3872	
	$4F(\frac{3}{2}^-)$	0.699	1.262	4010	
0 3 3 1 2	$1F(\frac{5}{2}^-)$	0.678	1.031	3428	3408
	$2F(\frac{5}{2}^-)$	0.744	1.474	3748	
	$3F(\frac{5}{2}^-)$	1.140	1.101	3876	
	$4F(\frac{5}{2}^-)$	0.698	1.243	4020	
0 3 3 1 3	$1F(\frac{5}{2}^-)$	0.676	1.022	3424	3394
	$2F(\frac{5}{2}^-)$	0.742	1.454	3744	
	$3F(\frac{5}{2}^-)$	1.136	1.096	3872	
	$4F(\frac{5}{2}^-)$	0.699	1.263	4009	
0 3 3 1 3	$1F(\frac{7}{2}^-)$	0.678	1.031	3428	3393
	$2F(\frac{7}{2}^-)$	0.744	1.475	3748	
	$3F(\frac{7}{2}^-)$	1.140	1.101	3876	
	$4F(\frac{7}{2}^-)$	0.698	1.242	4021	
0 3 3 1 4	$1F(\frac{7}{2}^-)$	0.676	1.021	3423	3373
	$2F(\frac{7}{2}^-)$	0.742	1.453	3744	
	$3F(\frac{7}{2}^-)$	1.136	1.095	3872	
	$4F(\frac{7}{2}^-)$	0.699	1.264	4009	
0 3 3 1 4	$1F(\frac{9}{2}^-)$	0.678	1.032	3428	3357
	$2F(\frac{9}{2}^-)$	0.744	1.476	3749	
	$3F(\frac{9}{2}^-)$	1.140	1.102	3876	
	$4F(\frac{9}{2}^-)$	0.698	1.241	4021	



TABLE IV: The root mean square radius (fm) and the mass spectrum (MeV) of the  $\Xi_b$  family.

$l_\rho \ l_\lambda \ L \ s \ j$	$nL(J^P)$	$\langle r_\rho^2 \rangle^{1/2}$	$\langle r_\lambda^2 \rangle^{1/2}$	mass	exp.[30]	[58]
0 0 0 0 0	$1S(\frac{1}{2}^+)$	0.518	0.400	5806	$\Xi_b^-$ 5797.0(0.6) $\Xi_b^0$ 5791.9(0.5)	5803
	$2S(\frac{1}{2}^+)$	0.607	0.705	6224		6266
	$3S(\frac{1}{2}^+)$	0.990	0.549	6480		6601
	$4S(\frac{1}{2}^+)$	0.672	1.066	6568		6913
0 1 1 0 1	$1P(\frac{1}{2}^-)$	0.539	0.571	6084		6120
	$2P(\frac{1}{2}^-)$	0.586	0.844	6421		6496
	$3P(\frac{1}{2}^-)$	1.034	0.713	6690		6805
	$4P(\frac{1}{2}^-)$	0.673	1.281	6732		7068
0 1 1 0 1	$1P(\frac{3}{2}^-)$	0.543	0.583	6097	6100.3(0.6)	6130
	$2P(\frac{3}{2}^-)$	0.585	0.853	6432		6502
	$3P(\frac{3}{2}^-)$	1.043	0.719	6700		6810
	$4P(\frac{3}{2}^-)$	0.668	1.293	6739		7073
0 2 2 0 2	$1D(\frac{3}{2}^+)$	0.551	0.743	6320		6366
	$2D(\frac{3}{2}^+)$	0.568	0.962	6613		6690
	$3D(\frac{3}{2}^+)$	0.990	1.040	6883		6966
	$4D(\frac{3}{2}^+)$	0.778	1.359	6890		7208
0 2 2 0 2	$1D(\frac{5}{2}^+)$	0.553	0.751	6327		6373
	$2D(\frac{5}{2}^+)$	0.568	0.967	6621		6696
	$3D(\frac{5}{2}^+)$	0.948	1.124	6888		6970
	$4D(\frac{5}{2}^+)$	0.831	1.294	6894		7212
0 3 3 0 3	$1F(\frac{5}{2}^-)$	0.555	0.903	6518		6577
	$2F(\frac{5}{2}^-)$	0.553	1.064	6795		6863
	$3F(\frac{5}{2}^-)$	0.619	1.646	7032		7114
	$4F(\frac{5}{2}^-)$	1.110	0.960	7057		7339
0 3 3 0 3	$1F(\frac{7}{2}^-)$	0.556	0.909	6523		6581
	$2F(\frac{7}{2}^-)$	0.553	1.070	6801		6867
	$3F(\frac{7}{2}^-)$	0.618	1.641	7034		7117
	$4F(\frac{7}{2}^-)$	1.111	0.965	7060		7342
0 4 4 0 4	$1G(\frac{7}{2}^+)$	0.554	1.048	6692		6760
	$2G(\frac{7}{2}^+)$	0.542	1.178	6970		7020
	$3G(\frac{7}{2}^+)$	0.607	1.745	7167		
	$4G(\frac{7}{2}^+)$	1.119	1.095	7214		
0 4 4 0 4	$1G(\frac{9}{2}^+)$	0.555	1.052	6695		6762
	$2G(\frac{9}{2}^+)$	0.544	1.189	6975		7032
	$3G(\frac{9}{2}^+)$	0.605	1.737	7169		
	$4G(\frac{9}{2}^+)$	1.120	1.098	7217		

TABLE V: The root mean square radius (fm) and the mass spectrum (MeV) of the  $\Xi'_b$  family (Part I).

$l_\rho \ l_\lambda \ L \ s \ j$	$nL(J^P)$	$\langle r_\rho^2 \rangle^{1/2}$	$\langle r_\lambda^2 \rangle^{1/2}$	mass	exp.[30]	[58]
0 0 0 1 1	$1S(\frac{1}{2}^+)$	0.604	0.411	5943	5935.02(0.05)	5936
	$2S(\frac{1}{2}^+)$	0.741	0.697	6350		6329
	$3S(\frac{1}{2}^+)$	0.998	0.559	6535		6687
	$4S(\frac{1}{2}^+)$	0.804	1.063	6691		6978
0 0 0 1 1	$1S(\frac{3}{2}^+)$	0.614	0.431	5971	5952.3(0.6) 5955.33(0.13)	5963
	$2S(\frac{3}{2}^+)$	0.735	0.716	6370		6342
	$3S(\frac{3}{2}^+)$	1.017	0.566	6554		6695
	$4S(\frac{3}{2}^+)$	0.793	1.087	6705		6984
0 1 1 1 0	$1P(\frac{1}{2}^-)$	0.642	0.608	6238		6233
	$2P(\frac{1}{2}^-)$	0.709	0.866	6569		6611
	$3P(\frac{1}{2}^-)$	1.074	0.705	6758		6915
	$4P(\frac{1}{2}^-)$	0.772	1.296	6866		7174
0 1 1 1 1	$1P(\frac{1}{2}^-)$	0.640	0.603	6232		6227
	$2P(\frac{1}{2}^-)$	0.709	0.862	6564		6604
	$3P(\frac{1}{2}^-)$	1.071	0.701	6754		6904
	$4P(\frac{1}{2}^-)$	0.774	1.292	6863		7164
0 1 1 1 1	$1P(\frac{3}{2}^-)$	0.643	0.610	6240		6234
	$2P(\frac{3}{2}^-)$	0.709	0.868	6572		6605
	$3P(\frac{3}{2}^-)$	1.076	0.707	6760		6905
	$4P(\frac{3}{2}^-)$	0.771	1.297	6868		7163
0 1 1 1 2	$1P(\frac{3}{2}^-)$	0.639	0.600	6229	6227.9(0.9)? 6226.8(1.6)?	6224
	$2P(\frac{3}{2}^-)$	0.709	0.859	6562		6598
	$3P(\frac{3}{2}^-)$	1.069	0.700	6752		6900
	$4P(\frac{3}{2}^-)$	0.774	1.291	6861		7159
0 1 1 1 2	$1P(\frac{5}{2}^-)$	0.644	0.613	6243		6226
	$2P(\frac{5}{2}^-)$	0.708	0.871	6574		6596
	$3P(\frac{5}{2}^-)$	1.077	0.708	6762		6897
	$4P(\frac{5}{2}^-)$	0.770	1.299	6869		7156
0 2 2 1 1	$1D(\frac{1}{2}^+)$	0.656	0.773	6460		6447
	$2D(\frac{1}{2}^+)$	0.690	0.992	6757		6767
	$3D(\frac{1}{2}^+)$	1.109	0.845	6941		
	$4D(\frac{1}{2}^+)$	0.754	1.464	7017		
0 2 2 1 1	$1D(\frac{3}{2}^+)$	0.658	0.780	6466		6459
	$2D(\frac{3}{2}^+)$	0.690	0.998	6763		6775
	$3D(\frac{3}{2}^+)$	1.111	0.850	6946		
	$4D(\frac{3}{2}^+)$	0.751	1.462	7020		

TABLE VI: The root mean square radius (fm) and the mass spectrum (MeV) of the  $\Xi'_b$  family (Part II).

$l_\rho \ l_\lambda \ L \ s \ j$	$nL(J^P)$	$\langle r_\rho^2 \rangle^{1/2}$	$\langle r_\lambda^2 \rangle^{1/2}$	mass	[58]
0 2 2 1 2	$1D(\frac{3}{2}^+)$	0.656	0.773	6460	6431
	$2D(\frac{3}{2}^+)$	0.690	0.992	6758	6751
	$3D(\frac{3}{2}^+)$	1.109	0.845	6941	
	$4D(\frac{3}{2}^+)$	0.754	1.464	7017	
0 2 2 1 2	$1D(\frac{5}{2}^+)$	0.658	0.780	6466	6432
	$2D(\frac{5}{2}^+)$	0.690	0.999	6764	6751
	$3D(\frac{5}{2}^+)$	1.112	0.851	6946	
	$4D(\frac{5}{2}^+)$	0.751	1.462	7021	
0 2 2 1 3	$1D(\frac{5}{2}^+)$	0.656	0.773	6460	6420
	$2D(\frac{5}{2}^+)$	0.690	0.991	6757	6740
	$3D(\frac{5}{2}^+)$	1.108	0.844	6941	
	$4D(\frac{5}{2}^+)$	0.754	1.464	7017	
0 2 2 1 3	$1D(\frac{7}{2}^+)$	0.658	0.781	6467	6414
	$2D(\frac{7}{2}^+)$	0.690	1.000	6765	6736
	$3D(\frac{7}{2}^+)$	1.112	0.851	6946	
	$4D(\frac{7}{2}^+)$	0.751	1.461	7021	
0 3 3 1 2	$1F(\frac{3}{2}^-)$	0.663	0.931	6657	6675
	$2F(\frac{3}{2}^-)$	0.678	1.121	6942	
	$3F(\frac{3}{2}^-)$	1.130	0.986	7110	
	$4F(\frac{3}{2}^-)$	0.734	1.580	7162	
0 3 3 1 2	$1F(\frac{5}{2}^-)$	0.664	0.936	6660	6686
	$2F(\frac{5}{2}^-)$	0.680	1.130	6946	
	$3F(\frac{5}{2}^-)$	1.131	0.991	7114	
	$4F(\frac{5}{2}^-)$	0.732	1.573	7164	
0 3 3 1 3	$1F(\frac{5}{2}^-)$	0.663	0.931	6657	6640
	$2F(\frac{5}{2}^-)$	0.678	1.121	6942	
	$3F(\frac{5}{2}^-)$	1.130	0.986	7110	
	$4F(\frac{5}{2}^-)$	0.734	1.580	7162	
0 3 3 1 3	$1F(\frac{7}{2}^-)$	0.664	0.936	6660	6641
	$2F(\frac{7}{2}^-)$	0.680	1.131	6947	
	$3F(\frac{7}{2}^-)$	1.131	0.991	7114	
	$4F(\frac{7}{2}^-)$	0.731	1.572	7165	
0 3 3 1 4	$1F(\frac{7}{2}^-)$	0.663	0.931	6657	6619
	$2F(\frac{7}{2}^-)$	0.678	1.121	6942	
	$3F(\frac{7}{2}^-)$	1.130	0.986	7110	
	$4F(\frac{7}{2}^-)$	0.734	1.580	7162	
0 3 3 1 4	$1F(\frac{9}{2}^-)$	0.664	0.937	6661	6610
	$2F(\frac{9}{2}^-)$	0.680	1.132	6947	
	$3F(\frac{9}{2}^-)$	1.131	0.991	7114	
	$4F(\frac{9}{2}^-)$	0.731	1.572	7165	

TABLE VII: Fitted values for the slope and intercept of the Regge trajectories for the  $\Xi_c$  and  $\Xi'_c$  families.

Trajectory	$n = 1$		$n = 2$		$n = 3$	
	$\alpha(\text{GeV}^2)$	$\beta(\text{GeV}^2)$	$\alpha(\text{GeV}^2)$	$\beta(\text{GeV}^2)$	$\alpha(\text{GeV}^2)$	$\beta(\text{GeV}^2)$
$\bar{3}_F(NP)(NJ)$	$1.493 \pm 0.056$	$5.580 \pm 0.160$	$1.433 \pm 0.022$	$8.047 \pm 0.063$	$1.507 \pm 0.032$	$9.305 \pm 0.091$
$\bar{3}_F(UP)(UJ)$	$1.456 \pm 0.043$	$7.122 \pm 0.098$	$1.446 \pm 0.023$	$9.399 \pm 0.052$	$1.501 \pm 0.026$	$10.784 \pm 0.059$
$6_F(NP)(UJ)$	$1.592 \pm 0.058$	$6.098 \pm 0.166$	$1.530 \pm 0.033$	$8.611 \pm 0.096$	$1.539 \pm 0.031$	$9.574 \pm 0.089$
$6_F(UP)(UJ)$	$1.487 \pm 0.033$	$7.959 \pm 0.076$	$1.473 \pm 0.026$	$10.292 \pm 0.059$	$1.482 \pm 0.018$	$11.260 \pm 0.041$
$6_F(NP)(UJ)$	$1.433 \pm 0.026$	$9.545 \pm 0.044$	$1.433 \pm 0.026$	$11.837 \pm 0.045$	$1.453 \pm 0.015$	$12.795 \pm 0.026$
$6_F(UP)(NJ)$	$1.507 \pm 0.040$	$4.933 \pm 0.153$	$1.459 \pm 0.022$	$7.451 \pm 0.082$	$1.474 \pm 0.019$	$8.371 \pm 0.071$
$6_F(NP)(NJ)$	$1.455 \pm 0.031$	$6.618 \pm 0.098$	$1.437 \pm 0.025$	$8.980 \pm 0.079$	$1.454 \pm 0.018$	$9.911 \pm 0.058$
$6_F(UP)(NJ)$	$1.463 \pm 0.034$	$8.041 \pm 0.078$	$1.444 \pm 0.025$	$10.383 \pm 0.057$	$1.460 \pm 0.019$	$11.336 \pm 0.043$

TABLE VIII: Fitted values for the slope and intercept of the Regge trajectories for the  $\Xi_b$  and  $\Xi'_b$  families.

Trajectory	$n = 1$		$n = 2$		$n = 3$	
	$\alpha(\text{GeV}^2)$	$\beta(\text{GeV}^2)$	$\alpha(\text{GeV}^2)$	$\beta(\text{GeV}^2)$	$\alpha(\text{GeV}^2)$	$\beta(\text{GeV}^2)$
$\bar{3}_F(NP)(NJ)$	$2.760 \pm 0.134$	$32.756 \pm 0.386$	$2.470 \pm 0.027$	$37.595 \pm 0.077$	$2.341 \pm 0.122$	$41.187 \pm 0.350$
$\bar{3}_F(UP)(UJ)$	$2.582 \pm 0.099$	$35.891 \pm 0.226$	$2.449 \pm 0.014$	$40.029 \pm 0.033$	$2.190 \pm 0.114$	$43.86 \pm 0.262$
$6_F(NP)(UJ)$	$2.820 \pm 0.129$	$34.316 \pm 0.371$	$2.592 \pm 0.032$	$39.116 \pm 0.092$	$2.518 \pm 0.076$	$41.681 \pm 0.219$
$6_F(UP)(UJ)$	$2.605 \pm 0.087$	$37.677 \pm 0.199$	$2.529 \pm 0.014$	$41.849 \pm 0.033$	$2.388 \pm 0.051$	$44.509 \pm 0.116$
$6_F(NP)(UJ)$	$2.465 \pm 0.068$	$40.538 \pm 0.117$	$2.512 \pm 0.013$	$44.409 \pm 0.022$	$2.309 \pm 0.038$	$47.045 \pm 0.065$
$6_F(UP)(NJ)$	$2.747 \pm 0.113$	$31.888 \pm 0.428$	$2.536 \pm 0.019$	$36.834 \pm 0.072$	$2.462 \pm 0.062$	$39.454 \pm 0.235$
$6_F(NP)(NJ)$	$2.580 \pm 0.085$	$35.207 \pm 0.273$	$2.510 \pm 0.016$	$39.450 \pm 0.050$	$2.374 \pm 0.053$	$42.222 \pm 0.170$
$6_F(UP)(NJ)$	$2.588 \pm 0.089$	$37.766 \pm 0.205$	$2.522 \pm 0.018$	$41.921 \pm 0.041$	$2.382 \pm 0.057$	$44.573 \pm 0.131$

TABLE IX: Mass spectrum shells of the  $\Xi'_c$  (top half) and  $\Xi_c$  (bottom half) families and masses are measured in MeV.

$nL$	$J = 1/2$	$J = 3/2$	$J = 5/2$	$J = 7/2$	$\langle r_\rho^2 \rangle^{1/2}$ (fm)	$\langle r_\lambda^2 \rangle^{1/2}$ (fm)
$2P$	3315 3326	3310 3331	3335		$0.76 \sim 0.77$	$0.96 \sim 0.99$
$3S$	3201	3244			$\sim 0.92$	$\sim 0.67$
$1D$	3201	3201 3211	3200 3211	3213	$0.66 \sim 0.67$	$0.85 \sim 0.87$
$2S$	3046 ( $\Xi_c(3055)?$ )	3095 ( $\Xi_c(3080)?$ )			$0.80 \sim 0.82$	$0.71 \sim 0.76$
$1P$	2941 ( $\Xi'_c(2939)?$ ) 2952 ( $\Xi'_c(2939)?$ )	2934 ( $\Xi'_c(2923)?$ ) 2958 ( $\Xi'_c(2964)?$ )	2964 ( $\Xi'_c(2964)?$ )		$0.64 \sim 0.65$	$0.65 \sim 0.68$
$1S$	<b>2590</b> ( $\Xi_c^{+,0}$ )	<b>2658</b> ( $\Xi'_c(2645)$ )			$0.59 \sim 0.61$	$0.43 \sim 0.48$
$1F$			3289		$\sim 0.57$	$\sim 1.00$
$2P$	3176	3199			$0.61 \sim 0.62$	$0.94 \sim 0.98$
$3S$	3155 ( $\Xi_c(3123)?$ )				$\sim 0.97$	$\sim 0.61$
$1D$		3063	3076		$0.56 \sim 0.57$	$0.82 \sim 0.85$
$2S$	2949 ( $\Xi_c(2970)$ )				$\sim 0.65$	$\sim 0.77$
$1P$	<b>2789</b> ( $\Xi_c(2790)$ )	<b>2819</b> ( $\Xi_c(2815)$ )			$0.54 \sim 0.55$	$0.62 \sim 0.66$
$1S$	<b>2479</b> ( $\Xi_c^{+,0}$ )				$\sim 0.51$	$\sim 0.44$

TABLE X: Mass spectrum shells of the  $\Xi'_b$  (top half) and  $\Xi_b$  (bottom half) families and masses are measured in MeV.

$nL$	$J = 1/2$	$J = 3/2$	$J = 5/2$	$J = 7/2$	$\langle r_\rho^2 \rangle^{1/2}$ (fm)	$\langle r_\lambda^2 \rangle^{1/2}$ (fm)
$1F$				6657 6660	$0.66 \sim 0.67$	$0.93 \sim 0.94$
		6657	6660			
$2P$	6564 6569	6562 6572	6574		$0.70 \sim 0.71$	$0.86 \sim 0.87$
$3S$	6535	6554			$1.00 \sim 1.02$	$0.56 \sim 0.57$
$1D$			6460 6466	6467	$0.65 \sim 0.66$	$0.77 \sim 0.78$
	6460	6460 6466				
$2S$	6350	6370			$\sim 0.74$	$\sim 0.70$
$1P$		6229 ( $\Xi_b(6227)?$ ) 6240	6243		$0.63 \sim 0.64$	$0.60 \sim 0.61$
	6232 6238					
$1S$	<b>5943</b> ( $\Xi'_b(5935)$ )	<b>5971</b> ( $\Xi'_b(5955, 5945)$ )			$0.60 \sim 0.61$	$0.41 \sim 0.43$
$1F$			6518	6523	$0.55 \sim 0.56$	$0.90 \sim 0.91$
$3S$	6480				$\sim 0.99$	$\sim 0.55$
$2P$	6421	6432			$0.58 \sim 0.59$	$0.84 \sim 0.85$
$1D$		6320 ( $\Xi_b(6327)$ )	6327 ( $\Xi_b(6333)$ )		$0.55 \sim 0.56$	$0.74 \sim 0.75$
$2S$	6224 ( $\Xi_b(6227)?$ )				$\sim 0.61$	$\sim 0.71$
$1P$	6084	<b>6097</b> ( $\Xi_b^-(6100)$ )			$0.53 \sim 0.54$	$0.57 \sim 0.58$
$1S$	<b>5806</b> ( $\Xi_b^{0,-}$ )				$\sim 0.52$	$\sim 0.40$